Received: 20 September 2017 | Revised: 04 September 2018 | Accepted: 07 September 2018

DOI: 10.1002/qj.3403

RESEARCH ARTICLE

Quarterly Journal of the Royal Meteorological Society RMetS

Source term estimation of multi-specie atmospheric release of radiation from gamma dose rates

Ondřej Tichý[1] | Václav Šmídl[1] | Radek Hofman[1] | Nikolaos Evangeliou[2]

[1]Department of Adaptive Systems, The Czech Academy of Sciences, Institute of Information Theory and Automation, Prague 8, Czech Republic
[2]Department of Atmospheric and Climate Research, Norwegian Institute for Air Research (NILU), Kjeller, Norway

Correspondence
Ondřej Tichý, The Czech Academy of Sciences, Institute of Information Theory and Automation, Pod Vodárenskou Věží 4, Prague 8 18208, Czech Republic. Email: otichy@utia.cas.cz

Determination of a source term of an accidental release of radioactive material into the atmosphere is very important for evaluating emergency situations and their consequences. However, knowledge of the source term and its composition is typically vague and uncertain. One possible way to obtain the source term is inverse modeling in which an atmospheric transport model is combined with field measurements. The most accessible measurements are those from gamma dose rate (GDR) detectors. However, GDR measurements represent a sum of contribution from all nuclides from both plume and deposition which makes the problem particularly difficult. The same difficulty arises when the measurements can not distinguish contribution from another species in the release, such as nuclides attached to different particle sizes. We propose a Bayesian method for recovery of the source term from GDR measurements where a priori knowledge on ratios of different species is given in the form of bounds. This knowledge is incorporated into the model of covariance matrix of the source term. The Bayesian methodology allows to handle uncertain knowledge on the nuclide ratios as well as unknown temporal correlations of the source term. We evaluate and compare the proposed method with other state-of-the-art methods on a twin experiment of a non-stationary release of 16 nuclides from the Czech nuclear power plant Temelin being registered by the Austrian GDR monitoring network. Real-world validation of the approach is performed on the latest measurements of concentration and deposition of caesium-137 from the Chernobyl accident, where we estimate composition of the source term from different particle sizes (species). The estimated source term is in very good agreement with previously reported results and the calculated species ratios are supported by the available observations.

KEYWORDS

chernobyl accident, covariance matrix, gamma dose rate, inverse modeling, multi-species source term estimation, nuclear accident, nuclides ratios

1 | INTRODUCTION

Determination of the source term of an atmospheric release of radioactive material is very important for nuclear accident emergency. However, information about the source term is always incomplete and subject to many uncertainties. One possible approach to estimation of the source term is to combine field measurements together with an atmospheric transport model (Nisbet and Weiss, 2010). The most informative measurements are atmospheric activity concentrations, which can be measured for each nuclide. However, they need to be collected for a selected period, typically several hours or even days (Leelössy *et al.*, 2017). Another type of measurements are surface activities that can be measured using fallout for each nuclide and integrated over period of time, daily at the best as in the case of Fukushima (Saunier *et al.*, 2013; Leelössy *et al.*, 2018). Therefore, gamma dose rate (GDR) measurements are mostly adopted when rapid response is needed due to their availability (Katata *et al.*, 2012; Kovalets *et al.*, 2016). However,

they represent a challenge for the inversion method since its value is a sum of contributions from all nuclides forming the plume radiation and deposition radiation (Saunier *et al.*, 2013; Zhang *et al.*, 2017). This issue may arise even for single nuclide when it is attached to different specie for example with different particle sizes. Once again, the detector will measure only a sum of contributions from these individual sources.

A lot of effort has been spend on source term estimation methods, also known as inverse methods, including optimization methods, e.g., (Eckhardt *et al.*, 2008; Davoine and Bocquet, 2007), iterative ensemble Kalman filter (Zhang *et al.*, 2015), Monte Carlo methods, e.g., (Rajaona *et al.*, 2015; Liu *et al.*, 2017), maximum entropy principle , e.g. (Bocquet, 2005; 2007; 2008), and variational Bayesian methods, e.g. (Tichý *et al.*, 2016). The application area range from nuclear explosions (Issartel and Baverel, 2003) and accidents such as Chernobyl (Davoine and Bocquet, 2007; Evangeliou *et al.*, 2017) or Fukushima (Winiarek *et al.*, 2012; Stohl *et al.*, 2012; Liu *et al.*, 2017), accidental release of radioactive materials (Tichý *et al.*, 2017), to emissions of volcanic ash during volcanic eruptions (Kristiansen *et al.*, 2010; Stohl *et al.*, 2011). These methods were mainly tested in scenarios where the measurements correspond to one specie in the source term, such as concentration measurements of individual nuclides. The number of estimation techniques for multi-specie source terms with measurements of the sum of their contributions is much smaller since it is much more challenging problem due to uninformative measurements. An example of such methods is estimation of multi-nuclide source terms from GDR measurement (Saunier *et al.*, 2013; Kovalets *et al.*, 2016; Zhang *et al.*, 2017). The key ingredients for solution is prior information on the composition of the source term.

In the case of multi-nuclide source terms, prior assumptions on nuclide ratios and their treatment has been found to be important (Saunier *et al.*, 2013; Zhang *et al.*, 2017; Katata *et al.*, 2012). These can be obtained, e.g, from analysis of the nuclide composition of the active power plant (reactor inventory combined with assumptions on the accident type) or from a few available nuclide-specific activity concentration samples. However, a methodology to incorporate this information into the inverse methods remains a challenge. One possible means to approach this problem is to use prior nuclide ratios ranges which then constrain the optimization problem in the form of barrier protection functions (Saunier *et al.*, 2013). This formulation can be also seen as a convex optimization problem with nuclide ratios ranges forming constraints and with an optional regularization term such as Tikhonov (Golub *et al.*, 1999) or least absolute shrinkage and selection operator (LASSO) (Tibshirani, 1996). Optimization formulation was also used by Hofman *et al.* (2015) where a transport matrix is augmented using known nuclide ratios. Recently, a probabilistic approach has been adopted by Zhang *et al.* (2017) where the multi-nuclide source term is sequentially estimated with use of update of source term covariance using prior knowledge on nuclide ratios. Notably, uncertainties of the source term are also output of the method. However, these approaches are based on description of the ratio uncertainty in the form of the covariance matrix of a Gaussian distribution and their manual tuning. The choice of tuning coefficients may be problematic in emergency situations.

In this paper, we assume to have knowledge on the source term composition in the form of intervals of admissible ratios of the species as considered by Saunier *et al.* (2013). We approach the problem in a Bayesian way and view the specie ratios as unknown variable with the admissible interval defining support of their prior distribution. The parameters of the prior distributions are estimated together with the source term. The estimation of the model parameter is performed using the variational Bayes method, e.g. (Jordan *et al.*, 1999; Šmídl and Quinn, 2006), where iterative algorithm is derived. This approximative method is a computationally simple alternative to Monte Carlo sampling. The Monte Carlo approach to estimation of the source term from GDR has been presented e.g. by Šmídl and Hofman (2014) but only for a single nuclide scenario.

Validation of the inversion methods from GDR measurements is an issue because there is no tracer experiment. Hence, we design a realistic twin experiment to theoretically validate the proposed method. The source term consists of 16 nuclides released from the Czech nuclear power plant Temelin. The Lagrangian particle dispersion model Flexpart (Stohl *et al.*, 2005) was used as the atmospheric transport model which is forced by ECMWF Era-Interim meteorological fields. The topology of the Austrian radiation monitoring network comprising of 480 receptors was used to simulate the hypothetical measurements. The proposed method is compared with state-of-the-art methods including optimization formulation with Tikhonov and LASSO regularization, and the method by (Zhang *et al.*, 2017).

Real data sets, such as the Chernobyl and the Fukushima accidents, do not provide ground truth of the source term (Aliyu *et al.*, 2015), and most of the measurements is nuclide-specific (Evangeliou *et al.*, 2016). However, the Chernobyl source term is also composed from many species, since the nuclides are attached to different particles sizes (Evangeliou *et al.*, 2017). The fractions of different particle sizes in the total release (and thus their ratios) are approximately known from measurements (Malá *et al.*, 2013). In this paper, we use this data as a validation experiment, where we assume that the fractions of various particle sizes are not known and we estimate them jointly in the inversion problem. We show that the results of the proposed method are in good agreement with the findings of Malá *et al.* (2013).

2 | THEORY AND METHODS

We assume that the vector of measurements $\mathbf{y}$ can be explained by linear model, e.g., (Seibert and Frank, 2004),

$$\mathbf{y} = \mathbf{M}\mathbf{x}. \tag{1}$$

In this case, vector $\mathbf{y} \in \mathbf{R}^{p\times 1}$ contains the measurements; $\mathbf{M} \in \mathbf{R}^{p\times n}$ is a known source-receptor-sensitivity (SRS) matrix given by atmospheric transport model (Seibert and Frank, 2004), and $\mathbf{x} \in \mathbf{R}^{n\times 1}$ is the unknown source term vector. Note that $\mathbf{y}$ and $\mathbf{M}$ are prone to errors and cumulate uncertainties from measurements and the atmospheric transport model used for SRS calculations (including errors in the meteorological data used to drive the transport model). In the paper, we assume that the number of species is m and that the number of time point is q; hence, the length of the vector of the source term is $n = mq$. For clarity, we assume the composition of the source term $\mathbf{x}$ where activity rates of each specie is stored in column vector as $\mathbf{x} = \left[\mathbf{x}_1^T, \dots, \mathbf{x}_m^T\right]^T$, where source term of the kth specie is $\mathbf{x}_k = \left[x_{k,1}, \dots, x_{k,q}\right]^T$ for each $k = 1, \dots, m$.

The sensors measure only sum of contributions from different species. Separation of the species can be achieved only from their different atmospheric transportation properties or from different physical half-life in the case of nuclides. These effects are reflected in the SRS matrix, however, they are very weak and simple solution using least square method, $\mathbf{x}_{\mathrm{LS}} = \left(\mathbf{M}^T\mathbf{M}\right)^{-1}\mathbf{M}^T\mathbf{y}$, fails since the problem is highly ill-posed. Therefore, we aim to use additional information on ratios of the kth specie in relation with the mth specie which can be expressed for each time step t similarly to Saunier *et al.* (2013) as

$$a_{k,t} \le \frac{x_{k,t}}{x_{m,t}} \le b_{k,t},\ \forall k = 1, \dots, m-1,\ \forall t = 1, \dots, q, \tag{2}$$

where $a_{k,t}$ and $b_{k,t}$ are known boundaries of the ratios. The limits may be time-dependent or constant for the whole release depending on available information.

2.1 | Relation of cost optimization and Bayesian approach

A wide range of papers based on linear model Equation 1 where the problem is formulated as an minimization problem has been published, see e.g. (Seibert, 2000; Seibert and Frank, 2004; Eckhardt *et al.*, 2008). The task is to minimize the cost function J,

$$J = (\mathbf{y} - \mathbf{M}\mathbf{x})^T \sigma_0^{-2} (\mathbf{y} - \mathbf{M}\mathbf{x}) + \mathbf{x}^T \mathrm{diag}\left(\boldsymbol{\sigma}_{\mathbf{x}}^{-2}\right)\mathbf{x}, \tag{3}$$

where the first term models the deviation of the model from the observation with standard observation and model error σ_0 and the second term penalizes higher values of the source term $\mathbf{x}$ with error standard deviation in vector $\boldsymbol{\sigma}_{\mathbf{x}}$ where symbol diag() denotes square diagonal matrix with argument vector on its diagonal and zeros otherwise. Then, the minimization problem can be written as $\mathbf{x}^* = \arg\min_{\mathbf{x}} J$.

This minimization problem can be interpreted as a maximum a posteriori estimate of the following probabilistic model

$$p(\mathbf{y}|\mathbf{x}) = \mathcal{N}\left(\mathbf{M}\mathbf{x}, \sigma_0^2\mathbf{I}_p\right) \propto e^{\left(-\frac{1}{2}(\mathbf{y}-\mathbf{M}\mathbf{x})^T\sigma_0^{-2}(\mathbf{y}-\mathbf{M}\mathbf{x})\right)}, \tag{4}$$

$$p(\mathbf{x}) = \mathcal{N}\left(\mathbf{0}, \mathrm{diag}\left(\boldsymbol{\sigma}_{\mathbf{x}}^2\right)\right) \propto e^{\left(-\frac{1}{2}\mathbf{x}^T\mathrm{diag}\left(\boldsymbol{\sigma}_{\mathbf{x}}^{-2}\right)\mathbf{x}\right)}, \tag{5}$$

where $\mathcal{N}$ denotes Gaussian (normal) distribution with given mean and covariance and $\mathbf{I}_p$ denotes identity matrix of the size given in the subscript and symbol $\propto$ denotes equality up to normalizing constant. The logarithm of the posterior probability of the unknown source term $\mathbf{x}$ is

$$\log p(\mathbf{x}|\mathbf{y}) = -\frac{1}{2}J + c, \tag{6}$$

where c aggregates constants independent of $\mathbf{x}$. Thus, maximization of log-likelihood Equation 6 is equivalent to minimization of the cost function Equation 3. In the basic maximum likelihood approach, the parameters σ_0 and $\boldsymbol{\sigma}_{\mathbf{x}}$ are treated as tuning parameters and are often chosen manually.

However, in the full Bayesian approach, parameters σ_0 and $\boldsymbol{\sigma}_{\mathbf{x}}$ can be considered to be unknown. After selection of their prior distributions, they can be estimated from the data. Using this principle, many more parameters can be relaxed, including unknown correlations in the prior covariance matrix (Tichý *et al.*, 2016).

2.2 | Proposed Bayesian formulation of linear inverse problem

Here, we formulate the probabilistic model of the multi-specie release where information on their ratios can be incorporated into the covariance matrix of the source term.

The observation model is identical to Equation 4 where isotropic Gaussian noise model is assumed. Here, we consider equivalent formulation with the precision (inverse variance) parametrized by ω, i.e. $\omega^{-1} = \sigma_0^2$, as

$$p(\mathbf{y}|\mathbf{x}, \omega) = \mathcal{N}\left(\mathbf{M}\mathbf{x}, \omega^{-1}\mathbf{I}_p\right), \tag{7}$$

The parameter ω is considered to be unknown and therefore subject to estimation; hence, we define its own prior distribution in the form of Gamma distribution similarly to (Winiarek *et al.*, 2011), which is conjugate for estimation of precision of the Gaussian distribution, as

$$p(\omega) = \mathcal{G}(\vartheta_0, \rho_0). \tag{8}$$

Here, $\mathcal{G}$ denotes the Gamma distribution and ϑ_0, ρ_0 are prior constants. When these constants are equal to zero, the prior becomes non-informative Jeffrey's prior. However, we recommend to set them to a small number such as 10^{-10} since the resulting algorithms is more numerically stable, as can be seen from Eqtions 65–66. The same recommendation is valid for all subsequent prior constants of Gamma distributions.

The main novelty of the proposed model is its model of the source term. The model is based on a special role of a

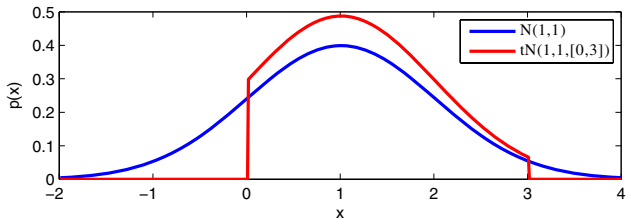

FIGURE 1 Example of the normal distribution $\mathcal{N}(1,1)$, blue line, and the truncated normal distribution $\mathcal{N}^{\mathrm{tr}}(1,1,[0,3])$, red line. Truncated normal distribution, see definition in Appendix 5, allows to analytically compute moments of normal distribution truncated to a specific interval [Colour figure can be viewed at wileyonlinelibrary.com]

selected specie denoted $\mathbf{x}_m$ (the last sub-vector in vector $\mathbf{x}$). This specie is modelled independently. We use the smooth and sparse prior by Tichý *et al.* (2016), i.e. prior model

$$p(x_{m,t}|x_{m,t-1}) = \mathcal{N}^{\mathrm{tr}}\left(l_{m,t}x_{m,t-1}, \upsilon_t^{-1}, [0,\infty]\right), \quad (9)$$

$$p(l_{m,t}|\psi_{m,t}) = \mathcal{N}\left(l_0, \psi_{m,t}^{-1}\right), \quad (10)$$

$$p\left(\psi_{m,t}\right) = \mathcal{G}\left(\zeta_0, \eta_0\right), \; t = 2,\dots,q, \quad (11)$$

$$p(\upsilon_t) = \mathcal{G}\left(\alpha_0, \beta_0\right), \; t = 1,\dots,q, \quad (12)$$

where symbol $\mathcal{N}^{\mathrm{tr}}$ denotes truncated Normal distribution with given support, see Appendix 5 and Figure 1, and where $l_{m,t}$, υ_t and $\psi_{m,t}$ are estimated from the data. Note that since $x_{m,t}$ depends on $x_{m,t-1}$, the model Equation 9 holds only for $t = 2,\dots,q$ while for $t = 1$, we assume $p(x_{m,1}) = \mathcal{N}^{\mathrm{tr}}\left(0, \upsilon_1^{-1}, [0,\infty]\right)$. The model essentially states that the two subsequent elements of the source term are correlated with unknown coefficient l_m of which we know only prior mean l_0. In this study, we assume that $l_0 = 1$ to favour smooth solutions and ζ_0, η_0 are selected as 10^{-2} as suggested in Tichý *et al.* (2016). However, the model allows for abrupt changes if they are supported by the observations, see Tichý *et al.* (2016) for discussion. The prior constants α_0, β_0 are chosen as $\alpha_0 = \beta_0 = 10^{-10}$ to represent non-informative prior .

The remaining species are modelled using linear model of correlation. Multiplying Equation 2 by $x_{m,t}$, we can consider the constraint Equation 2 to be a constraint on a coefficient of linear regression:

$$x_{k,t} = l_{k,t}x_{m,t}, \quad a_{k,t} < l_{k,t} < b_{k,t}, \quad (13)$$

where $l_{k,t}$ is the regression coefficient. To allow for model inaccuracy, we propose to use the probabilistic model

$$p(x_{k,t}|x_{m,t}) = \mathcal{N}^{\mathrm{tr}}\left(l_{k,t}x_{m,t}, \upsilon_t^{-1}, [0,\infty]\right), \quad (14)$$

$$p(l_{k,t}|\psi_{k,t}) = \mathcal{N}^{\mathrm{tr}}\left(0, \psi_{k,t}^{-1}, [a_{k,t}, b_{k,t}]\right), \quad (15)$$

$$p\left(\psi_{k,t}\right) = \mathcal{G}\left(\kappa_0, \nu_0\right), \quad (16)$$

for $t = 1,\dots,q$, $k = 1,\dots,m-1$, where $l_{k,t}$, υ_t and $\psi_{k,t}$ will be also estimated from the data. Prior constants κ_0, ν_0 are selected non-informatively as 10^{-10}. Note that this is the same structure that is used for $\mathbf{x}_m$. Precision of model Equation 14 at time t is assumed to be the same for all elements of $x_{k,t}$ and $x_{m,t}$ using the same precision coefficient υ_t that is estimated from the data. A significant change from the model for $x_{m,t}$ is that the regression coefficient is a priori restricted to be within the prescribed bounds using the truncated Normal distribution in Equation 15.

Joining models Equations 9 and 14 we can write prior model of the full vector of unknowns $\mathbf{x}$, $\mathbf{x} = \left[\mathbf{x}_1^T, \dots, \mathbf{x}_m^T\right]^T$ to be:

$$p(\mathbf{x}|\mathbf{\Omega}) = \mathcal{N}^{\mathrm{tr}}\left(\mathbf{0}, \mathbf{\Omega}^{-1}, [0,+\infty]\right), \quad (17)$$

where $\mathbf{\Omega}$ denotes precision matrix. The precision matrix $\mathbf{\Omega}$ has a specific form:

$$\mathbf{\Omega} = \mathbf{L}\mathbf{\Upsilon}\mathbf{L}^T, \quad (18)$$

where $\mathbf{L}$ is a lower triangular matrix with structure

$$\mathbf{L} = \left(\begin{array}{c|c|c|c|c} \mathbf{I}_t & 0 & 0 & 0 & 0 \\ 0 & \mathbf{I}_t & 0 & 0 & 0 \\ 0 & 0 & \ddots & 0 & 0 \\ 0 & 0 & 0 & \mathbf{I}_t & 0 \\ \hline \mathbf{L}_1 & \mathbf{L}_2 & \cdots & \mathbf{L}_{m-1} & \mathbf{L}_m \end{array}\right), \quad (19)$$

where sub-matrices $\mathbf{L}_m$ and $\mathbf{L}_k$, $k = 1,\dots,m-1$, are composed of unknown regression coefficients of models Equations 9 and 14 as follows:

$$\mathbf{L}_m = \begin{pmatrix} 1 & 0 & 0 & 0 \\ -l_{m,1} & 1 & 0 & 0 \\ 0 & \ddots & \ddots & 0 \\ 0 & 0 & -l_{m,q-1} & 1 \end{pmatrix}, \quad (20)$$

$$\mathbf{L}_k = \begin{pmatrix} -l_{k,1} & 0 & 0 & 0 \\ 0 & -l_{k,2} & 0 & 0 \\ 0 & 0 & \ddots & 0 \\ 0 & 0 & 0 & -l_{k,q} \end{pmatrix}, \; k = 1,\dots,m-1 \quad (21)$$

The matrix $\mathbf{\Upsilon}$ is a diagonal matrix with positive entries on the diagonal. Similarly to the model of the matrix $\mathbf{L}$, we aim to model the matrix $\mathbf{\Upsilon}$ related to the mth specie. Again, we assume block structure of the matrix $\mathbf{\Upsilon}$ as

$$\mathbf{\Upsilon} = \left(\begin{array}{c|c|c|c} \mathbf{\Upsilon}_m & 0 & 0 & 0 \\ \hline 0 & \ddots & 0 & 0 \\ 0 & 0 & \mathbf{\Upsilon}_m & 0 \\ \hline 0 & 0 & 0 & \mathbf{\Upsilon}_m \end{array}\right), \quad (22)$$

where $\mathbf{\Upsilon}_m$ is diagonal matrix of the size q with diagonal entries are denoted as $\upsilon_1, \dots, \upsilon_q$.

2.2.1 | Variational Bayes solution

Estimation of all unknown model parameters can be done by the Bayes' rule. This task is, however, intractable. Therefore, we seek an approximate solution. Here, we employ the variational Bayes (VB) methodology (Jordan *et al.*, 1999; Šmídl and Quinn, 2006) where the posterior distributions are assumed in a specific form of conditional independence:

$$p\left(\mathbf{x}, \upsilon_t, l_{k,t}, \psi_{k,t}, \omega|\mathbf{y}\right) \approx p\left(\mathbf{x}|\mathbf{y}\right) p\left(\upsilon_t|\mathbf{y}\right) p\left(l_{k,t}|\mathbf{y}\right) p\left(\psi_{k,t}|\mathbf{y}\right) p\left(\omega|\mathbf{y}\right). \quad (23)$$

The best possible approximation can be obtained using minimization of Kullback-Leibler divergence (Kullback and Leibler, 1951) between the posteriors and the restricted from

of the solution. This minimization uniquely determines the forms of the posterior distributions as

$$\tilde{p}(\mathbf{x}|\mathbf{y}) = \mathcal{N}^{\mathrm{tr}}(\mu_{\mathbf{x}}, \Sigma_{\mathbf{x}}, [0, +\infty]), \quad (24)$$

$$\tilde{p}(\upsilon_t|\mathbf{y}) = \mathcal{G}(\alpha_t, \beta_t), \ t = 1, \dots, q, \quad (25)$$

$$\tilde{p}\left(l_{m,t}|\mathbf{y}\right) = \mathcal{N}\left(\mu_{l_{m,t}}, \Sigma_{l_{m,t}}\right), \ t = 1, \dots, q-1, \quad (26)$$

$$\tilde{p}\left(\psi_{m,t}|\mathbf{y}\right) = \mathcal{G}\left(\zeta_{m,t}, \eta_{m,t}\right), \ t = 1, \dots, q-1, \quad (27)$$

$$\tilde{p}\left(l_{k,t}|\mathbf{y}\right) = \mathcal{N}^{\mathrm{tr}}\left(\mu_{l_{k,t}}, \Sigma_{l_{k,t}}, [a_{k,t}, b_{k,t}]\right), \ t = 1, \dots, q, \quad (28)$$

$$\tilde{p}\left(\psi_{k,t}|\mathbf{y}\right) = \mathcal{G}\left(\kappa_{k,t}, \nu_{k,t}\right), \ t = 1, \dots, q, \quad (29)$$

$$\tilde{p}(\omega|\mathbf{y}) = \mathcal{G}(\vartheta, \rho), \quad (30)$$

for $k = 1, \dots, m-1$, where the shaping parameters $\mu_{\mathbf{x}}, \Sigma_{\mathbf{x}}, \alpha_t, \beta_t, \mu_{l_{m,t}}, \Sigma_{l_{m,t}}, \zeta_{m,t}, \eta_{m,t}, \mu_{l_{k,t}}, \Sigma_{l_{k,t}}, \kappa_{k,t}, \nu_{k,t}, \vartheta, \rho$ are derived using the VB method in Appendix 5. These shaping parameters are functions of standard moment of posterior distribution denoted, e.g., as $\langle \mathbf{x} \rangle$ where brackets $\langle . \rangle$ denotes expected value. The shaping parameters together with standard moments form a set of implicit equation which need to be solved iteratively. The first probability distribution evaluated in the iterations is Equation 24 with $\langle \mathbf{L} \rangle$ and $\langle \mathbf{\Upsilon} \rangle$ set to identity matrices and $\langle \omega \rangle = \frac{1}{\max \mathbf{M}^T\mathbf{M}}$. The remaining distributions are evaluated in the order of Equations 24–30. The resulting code can be downloaded from http://www.utia.cz/linear_inversion_methods.

Note that similarly to Zhang *et al.* (2017), the algorithm allows to sequential updates on receding (moving) window. Here, arbitrary subset of time-index $[1, \dots, t]$ can be considered for each specie at each moving step. However, to study this computational scheme is beyond the scope of this paper.

2.3 | Other methods for incorporation of ranges on ratios

2.3.1 | Convex optimization with constraints

The inverse problem Equation 1 together with constraints Equation 2 can be reformulated as an optimization problem. Ordinary minimization of the quadratic norm of $||\mathbf{y} - \mathbf{M}\mathbf{x}||_2^2$ yields typically poor results due to ill-conditioned matrix M; however, constraints and regularization terms can be employed to achieve more reliable results. In our case, the minimization problem is formulated as follows:

$$\mathbf{x}^* = \arg\min_{\mathbf{x}} \left\{ ||\mathbf{y} - \mathbf{M}\mathbf{x}||_2^2 + \alpha g(\mathbf{x}) \right\}, \quad \text{subject to } \mathbf{x} \geq 0, \ a_{k,t} \leq \frac{x_{k,t}}{x_{m,t}} \leq b_{k,t}, \ \forall k, \ \forall j, \quad (31)$$

where $\alpha > 0$ is selected weight of the regularization term $g(\mathbf{x})$, source term $\mathbf{x}$ is assumed to be positive and constrained according to Equation 2. We consider two regularization terms commonly used in literature, Tikhonov regularization, see (Golub *et al.*, 1999), and LASSO regularization, see (Tibshirani, 1996),

$$g_{\mathrm{Tikhonov}}(\mathbf{x}) = ||\mathbf{x}||_2^2, \quad (32)$$

$$g_{\mathrm{LASSO}}(\mathbf{x}) = ||\mathbf{x}||_1, \quad (33)$$

where $||\mathbf{x}||_1 = \sum_i |x_i|$ denotes l_1-norm of the vector $\mathbf{x}$. We stress that the solution strongly depends on the selection of the weight of the regularization, on the parameter α. In the following experiments, we select this parameter manually after considering many possible choices.

Since the optimization problem Equation 31 remains convex, we use the CVX toolbox (Grant *et al.*, 2008; Grant and Boyd, 2014) which is a Matlab toolbox where the problem Equation 31 can be implemented and solved.

2.3.2 | Sequential multi-nuclide emission rate estimation method

Recently, a method for sequential estimation of the source term composition and nuclide emission rates has been introduced by Zhang *et al.* (2017). The key is the minimization of the cost function of a regularized weighted least square problem

$$\mathbf{x}^* = \arg\min_{\mathbf{x}} \left[(\mathbf{y} - \mathbf{M}\mathbf{x})^T \mathbf{R}^{-1} (\mathbf{y} - \mathbf{M}\mathbf{x}) + \mathbf{x}^T \mathbf{B}_0^{-1} \mathbf{x} \right], \quad (34)$$

where $\mathbf{R}$ represents the error covariance matrix of measurement and $\mathbf{B}_0$ represents covariance matrix for the source term constructed using knowledge of nuclide ratios. At each time step i, the estimated source term is updated and recalculated with use of incoming measurement as

$$\mathbf{K}_i = \mathbf{B}_i \mathbf{M}_i^T \left(\mathbf{R}_i + \mathbf{M}_i \mathbf{B}_i \mathbf{M}_i^T \right)^{-1}, \quad (35)$$

$$\mathbf{x}_i = \begin{pmatrix} \mathbf{x}_{i-1} \\ \mathbf{x}_{0,i} \end{pmatrix} + \mathbf{K}_i \left(\mathbf{y}_i - \mathbf{M}_i \begin{pmatrix} \mathbf{x}_{i-1} \\ \mathbf{x}_{0,i} \end{pmatrix} \right), \quad (36)$$

where subscript i denotes sub-selection of part of respected measurement or variable related to time $1, \dots, i$ and $\mathbf{B}_i$ is composed of information on nuclide ratios and its uncertainties, see Zhang *et al.* (2017) for details. Since this inversion method may yield negative estimates in $\mathbf{x}$, suppression of these negative estimates are proposed using artificial observations with zero mean and large uncertainty. We use reference implementation provided by its authors online.

However, we stress that the original algorithm is suitable only for well conditioned problems since under realistic conditions, the inversion in Equation 35 may be ill-conditioned and numerically unstable as in our experiment. Therefore, we modified the Equation 35 using the regularization term as

$$\widetilde{\mathbf{K}}_i = \mathbf{B}_i \mathbf{M}_i^T \Big(\mathbf{R}_i + \mathbf{M}_i \mathbf{B}_i \mathbf{M}_i^T + \\ + \mathrm{norm}\left[\mathbf{R}_i + \mathbf{M}_i \mathbf{B}_i \mathbf{M}_i^T \right] I_{\mathrm{size}(\mathbf{R}_i)} \Big)^{-1} \quad (37)$$

where norm[ ] denotes the largest singular value of the given matrix. This regularization improve the results in the following experiments significantly. Nevertheless, we will refer to this method as Zhang_2017 in the following experiments.

Note on computational cost

The computational time of all methods is in the range of tens of seconds on standard PC for cases studied in this paper.

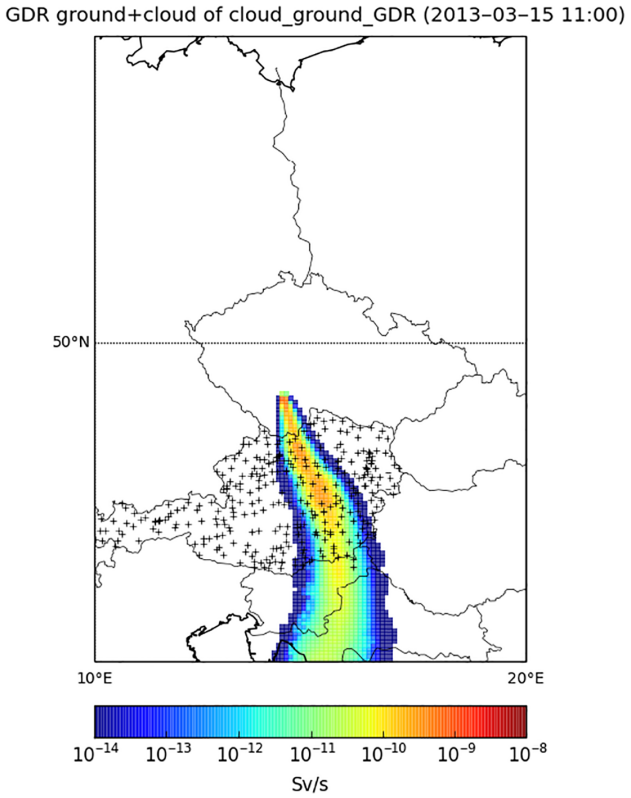

FIGURE 2 Gamma dose rate from the cloud shine and deposition 12 hr after the start of the release [Colour figure can be viewed at wileyonlinelibrary.com]

Exact runtimes vary with different settings and tuning parameters, different methods also use different numbers of cores on the used four-core CPU. Since none of the methods was optimized for execution speed, we provide only relative comparison. On average, the shortest runtimes has the method Zhang_2017 while the longest has the convex optimization via the CVX toolbox. The proposed method is between those two.

3 | TWIN EXPERIMENT OF MULTI-NUCLIDE RELEASE

In this section, we will use simulated twin experiment scenario, i.e. SRS matrix $\mathbf{M}$ and measurement vector $\mathbf{y}$ are simulated using a model.

3.1 | Twin experiment

For the purpose of this twin experiment, we use the source term designed by the Czech National Radiation Protection Institute (NRPI) for the Czech nuclear power plant Temelin. Here, the reactor type is Water-Water Energetic Reactor (VVER) delivering 1000 MW of electrical power (VVER-1000). For the purpose of testing dispersion models and nuclear safety assessment, the NIPR designed a simplified source term (Kuča *et al.*, 2012) consisting of 16

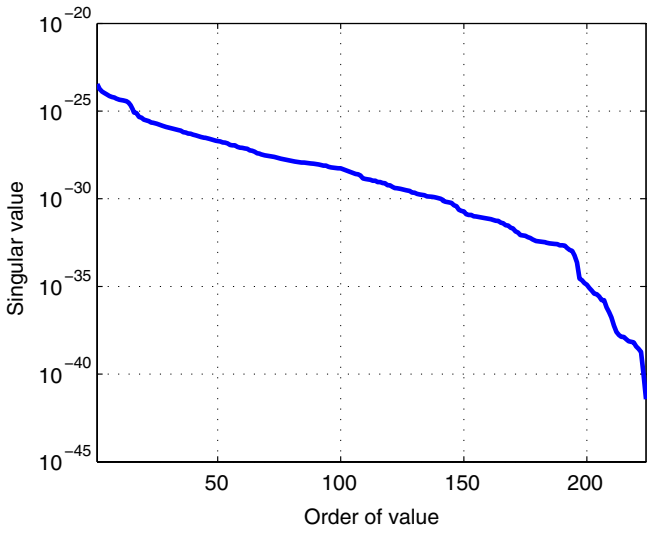

FIGURE 3 Plot of singular values of the SRS matrix M [Colour figure can be viewed at wileyonlinelibrary.com]

nuclides from the former RODOS source term (Savushkin *et al.*, 1998) called VVER1000-ST2 assuming severe accident of the VVER-1000 nuclear reactor with fuel melting, steam explosion, destruction of containment.

We follow the NIPR source term (Kuča *et al.*, 2012) and consider a simulated release of a mixture of 16 nuclides, $m = 16$: Cs-136, Cs-134, Cs-137, I-133, I-131, I-135, I-132, I-134, Kr-85m, Kr-88, Kr-87, Sr-90, Sr-89, Te-132, Xe-135, Xe-133 with details on the release given in Table 1. We assume the release to happen from an existing facility, namely the Czech nuclear power plant Temelin. We aim to reconstruct the release using topology of the Austrian radiation monitoring network comprising of 480 receptors, see Figure 2. We use the Lagrangian atmospheric dispersion model Flexpart 9.2 (FLEXible PARTicle dispersion model) (Stohl *et al.*, 1998; Stohl *et al.*, 2005) which is forced by the ECMWF Era-Interim meteorological fields (Dee *et al.*, 2011) with horizontal resolution 0.5°. Runs were done with convection turned on. Time resolution of both source and receptors was 1 hr. Calculations of the measurements were done in a nested grid with horizontal resolution approx 10×10 km (at the latitude of the source) whereas global mother grid had horizontal resolution 1×1 degree. We used three vertical output layers: 0–150, 150–500 and 500–2000 m. Every hour of the release is simulated using 500 000 particles from the stack with a given height above the ground in the first layer. The concentration and consequently the gamma dose rate at receptors is assumed to be that of the ground layer 0-150 m. In this experiment, the total time of measurement is 14 hr (with 6 hr release in the middle of the interval given in Table 1), $q = 14$, implying $\mathbf{y} \in R^{6720\times1}$ and $\mathbf{M} \in \mathbf{R}^{6720\times224}$. In this case, the condition number of the matrix $\mathbf{M}$ is 9.478×10^{17} and the plot of singular values of the matrix $\mathbf{M}$ is given in Figure 3 implying significantly ill-condition problem. The starting time of the simulation is selected on March 14, 2013 in 2300 UTC.

TABLE 1 The complete description of the simulated release of 16 nuclides. Note that in hours 1–4 and hours 11–14, zero activity release is considered

Nuclide	5h (Bq/h)	6h (Bq/h)	7h (Bq/h)	8h (Bq/h)	9h (Bq/h)	10h (Bq/h)
Kr-85m	3.33e13	4.66e16	2.68e15	2.68e15	2.68e15	2.68e15
Kr-87	7.03e15	9.84e16	5.63e15	5.63e15	5.63e15	5.63e15
Kr-88	1.04e14	1.45e16	8.30e15	8.30e15	8.30e15	8.30e15
Sr-89	4.49e12	1.35e16	5.63e14	5.63e14	5.63e14	5.63e14
Sr-90	4.82e11	1.45e15	6.03e13	6.03e13	6.03e13	6.03e13
I-131	1.57e14	1.10e16	3.15e15	3.15e15	3.15e15	3.15e15
I-132	2.28e14	1.60e16	4.55e15	4.55e15	4.55e15	4.55e15
I-133	3.20e14	2.24e16	6.40e15	6.40e15	6.40e15	6.40e15
I-134	3.51e14	2.46e16	7.00e15	7.00e15	7.00e15	7.00e15
I-135	3.00e14	2.10e16	6.00e15	6.00e15	6.00e15	6.00e15
Te-132	1.80e13	6.50e15	1.10e15	1.10e15	1.10e15	1.10e15
Cs-134	2.10e12	2.36e16	1.31e15	1.31e15	1.31e15	1.31e15
Cs-136	5.04e11	5.67e15	3.15e14	3.15e14	3.15e14	3.15e14
Cs-137	1.32e12	1.48e16	8.23e14	8.23e14	8.23e14	8.23e14
Xe-133	3.21e14	4.49e17	2.58e16	2.58e16	2.58e16	2.58e16
Xe-135	6.83e14	9.56e16	5.45e15	5.45e15	5.45e15	5.45e15

To save computational time, we propagate in Flexpart just two species (one for noble gases and one for particulates - we do not distinguish here between aerosol-bound and gaseous iodine since we do not consider it important here). The resulting matrices are converted to matrices for each nuclide by applying post-processing for radioactive decay with different physical half-life. . Gamma dose rate contribution from both cloudshine and groundshine is calculated. SRS matrix for activity concentration provided by FLEXPART is converted into SRS matrix for cloudshine using gamma dose rate conversion coefficients for semi-infinite cloud approximation. Similarly, deposited activity yielded by FLEXPART for particulates is converted into groundshine contribution using gamma dose conversion coefficients for infinite plane approximation. Dose conversion coefficients for both coudshine and groundshine are taken from (Joint working group of Radiation Protection Bureau, 1999).

In our twin experiment, the measurement vector $\mathbf{y}$ is corrupted by noise added to each element of $\mathbf{y}_{\text{exact}} = \mathbf{M}\mathbf{x}_{\text{true}}$. In reality, the measured value is a sum of activity from the release and a natural background radiation. We assume that the natural background radiation is $\mu_{\text{bg}} = 10^{-7}$ Sv/h (Šmídl and Hofman, 2014) with $\sigma_{\text{bg}} = 0.25 \times 10^{-7}$. Moreover, the radiation dose sensors are corrupted by error of measurement which is typically proportional to the measured gamma dose by the factor in the range 7–20% (Thompson *et al.*, 2000). Therefore, we assume five factors, denoted as noise levels, $e_{\text{level}} = \{1, 5, 10, 20, 30\}\%$. In summary,

$$\mathbf{y} \sim \mathcal{N}\left(\mathbf{y}_{\text{exact}} + \mu_{\text{bg}}, \sigma_{\text{bg}}^2 + (e_{\text{level}}\mathbf{y}_{\text{exact}})^2\right), \tag{38}$$

where negative elements of $\mathbf{y}$ are cropped to zero when occur. Since $\mathbf{y}_{\text{exact}}$ is not known, we approximate the variance of Equation 38 by the realization, i.e. $\text{cov}(\mathbf{y}) = \sigma_{\text{bg}}^2 + (e_{\text{level}}\mathbf{y})^2$. An illustration of the generated level of degradation is given in Figure 4 where scatter plot between $\mathbf{y}$ and $\mathbf{M}\mathbf{x}_{\text{true}}$ for each noise level is shown.

Nuclide ratios are the key additional information in this study. Although we know them exactly since we simulate the source term, we aim for much realistic approximate knowledge of nuclide ratios in the form of intervals Equation 2. For this, we calculate the exact ratios $\frac{x_{k,t}}{x_{m,t}}$ and assume boundaries $a_{k,t} = 0.5\frac{x_{k,t}}{x_{m,t}}$ and $b_{k,t} = 2.5\frac{x_{k,t}}{x_{m,t}}$. These intervals $[a_{k,t}, b_{k,t}]$ are inputs for the proposed algorithm, Section 2.2, and convex optimization algorithms, Section 2.3.1. Note that the selection of $a_{k,t}$ and $b_{k,t}$ may be too narrow and it is used only as an example and for validation purpose. In realistic release, the intervals may cover a few orders of magnitude Saunier *et al.* (2013). For the Zhang_2017 algorithm, we set the mean values to be equal to the exact ratios and standard deviations to be equal to these means as proposed in their implementation of the algorithm.

3.2 | Evaluation criteria

The use of the twin experiment described in Section 3.1 allow us to compare the estimated source terms from various inversion methods with the simulated ground truth source term from the twin experiment. The methods can be compared using statistical Monte Carlo studies for various realizations of the noise. We have selected the following statistical coefficients: figure of merit in space (FMS) (Abida and Bocquet, 2009), normalized mean square error (NMSE), and fractional bias (FB) (Chang and Hanna, 2004), which are standard parameters in evaluation of hazardous release models.

The figure of merit in space is defined as

$$\text{FMS} = \frac{\sum_{j=1}^{n} \min\left(\mathbf{x}_{\text{true},j}, \langle\mathbf{x}\rangle_j\right)}{\sum_{j=1}^{n} \max\left(\mathbf{x}_{\text{true},j}, \langle\mathbf{x}\rangle_j\right)} \tag{39}$$

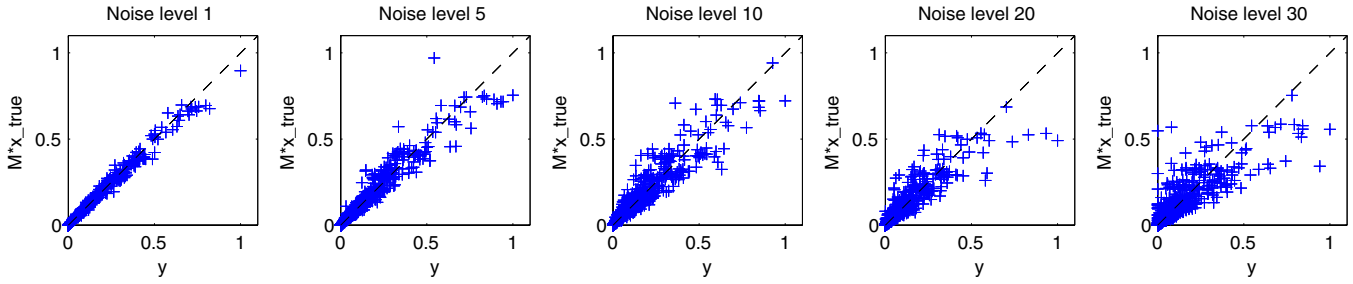

FIGURE 4 Scatter plots of $\mathbf{y}$ and $M\mathbf{x}_{\text{true}}$ for one realization of the noise for each noise level [Colour figure can be viewed at wileyonlinelibrary.com]

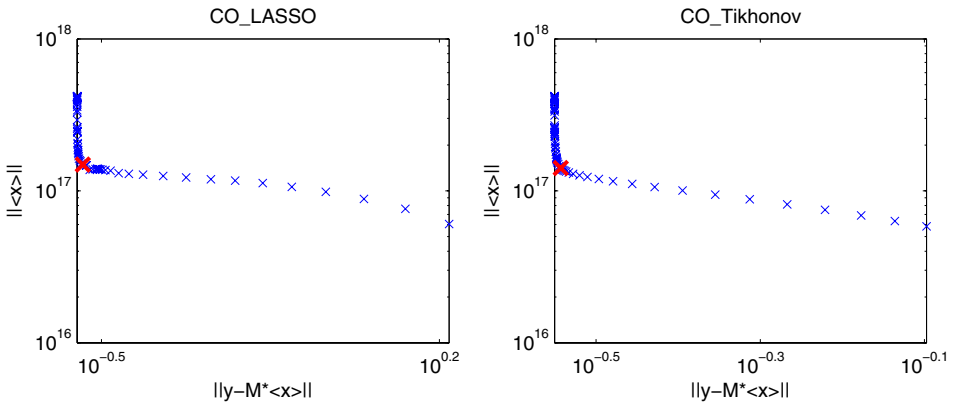

FIGURE 5 L-curves of the regularization parameters α for CO_LASSO and CO_Tikhonov methods. Red crosses denotes the selected parameter α for each method: $\alpha_{\text{LASSO}} = 10^{-2}$, $\alpha_{\text{Tikhonov}} = 10^{-2}$ [Colour figure can be viewed at wileyonlinelibrary.com]

and is classically used in space analysis where it is defined by the ratio between the intersection of the areas, and their union. This implies that higher values of FMS correspond to a better performance of the model. The normalized mean square error is defined as

$$\text{NMSE} = \frac{\frac{1}{n}\sum_{j=1}^{n}\left(\mathbf{x}_{\text{true},j} - \langle\mathbf{x}\rangle_j\right)^2}{\left(\frac{1}{n}\sum_{j=1}^{n}\mathbf{x}_{\text{true},j}\right)\left(\frac{1}{n}\sum_{j=1}^{n}\langle\mathbf{x}\rangle_j\right)}. \tag{40}$$

The NMSE criterion shows the most striking differences between the original source term and the model; hence, higher value of NMSE does not necessarily mean that the model is completely wrong. The fractional bias is defined as

$$\text{FB} = 2\frac{\frac{1}{n}\sum_{j=1}^{n}\mathbf{x}_{\text{true},j} - \frac{1}{n}\sum_{j=1}^{n}\langle\mathbf{x}\rangle_j}{\frac{1}{n}\sum_{j=1}^{n}\mathbf{x}_{\text{true},j} + \frac{1}{n}\sum_{j=1}^{n}\langle\mathbf{x}\rangle_j}, \tag{41}$$

so that FB $\in [-2, +2]$ where the ideal value is zero.

3.3 | Multi-nuclide source term estimation

Here, we demonstrate and discuss results of the studied methods on one particular realization of measurement vector $\mathbf{y}$ degraded by noise level of 10%. We aim to provide more intuitive comparison on a single example. Statistical comparison on multiple realizations will be given in the next section. The methods from Section 2 are used: convex optimization formulation with LASSO regularization term (denoted as CO_LASSO), convex optimization formulation with Tikhonov regularization term (denoted as CO_Tikhonov), the method by Zhang et al. (Zhang *et al.*, 2017) (denoted as Zhang_2017), and our proposed method. The CO_LASSO and CO_Tikhonov methods need to preselect the regularization parameter α. For this dataset, we propose the following selection: $\alpha_{\text{LASSO}} = 10^{-2}$ and $\alpha_{\text{Tikhonov}} = 10^{-2}$. These selections have been made based on the L-curve method (Hansen, 1992), see Figure 5, where plot of $\log||\langle\mathbf{x}\rangle||$ against $\log||\mathbf{y} - \mathbf{M}\langle\mathbf{x}\rangle||$ has been made and parameter α corresponding to elbow of the plot is selected.

The results from CO_LASSO and CO_Tikhonov methods are shown in Figure 6. The estimated CO_LASSO source term is displayed using blue line, the estimated CO_Tikhonov source term is displayed using green line, and the original source term, denoted as the ground truth, is displayed using dashed red line. The source term is given for each specific nuclide in subplots. Note that these two methods do not provide uncertainties on the estimated source term. In this particular realization of the noise, the timing of the source term is estimated well, however, this is not generally the case. The results from Zhang_2017 are given in Figure 7 where the estimated source term is displayed using blue line accompanied by the 99% highest posterior density region which is denoted by the green filled region. The original source term is displayed using dashed red line. Here, the original source term not always match with the estimated one; however, it is within uncertainty boundaries covering the original source term. Notably, the source term is estimated with huge uncertainty for all nuclides. The results from the proposed method are given in Figure 8 with the same line meanings as in the case

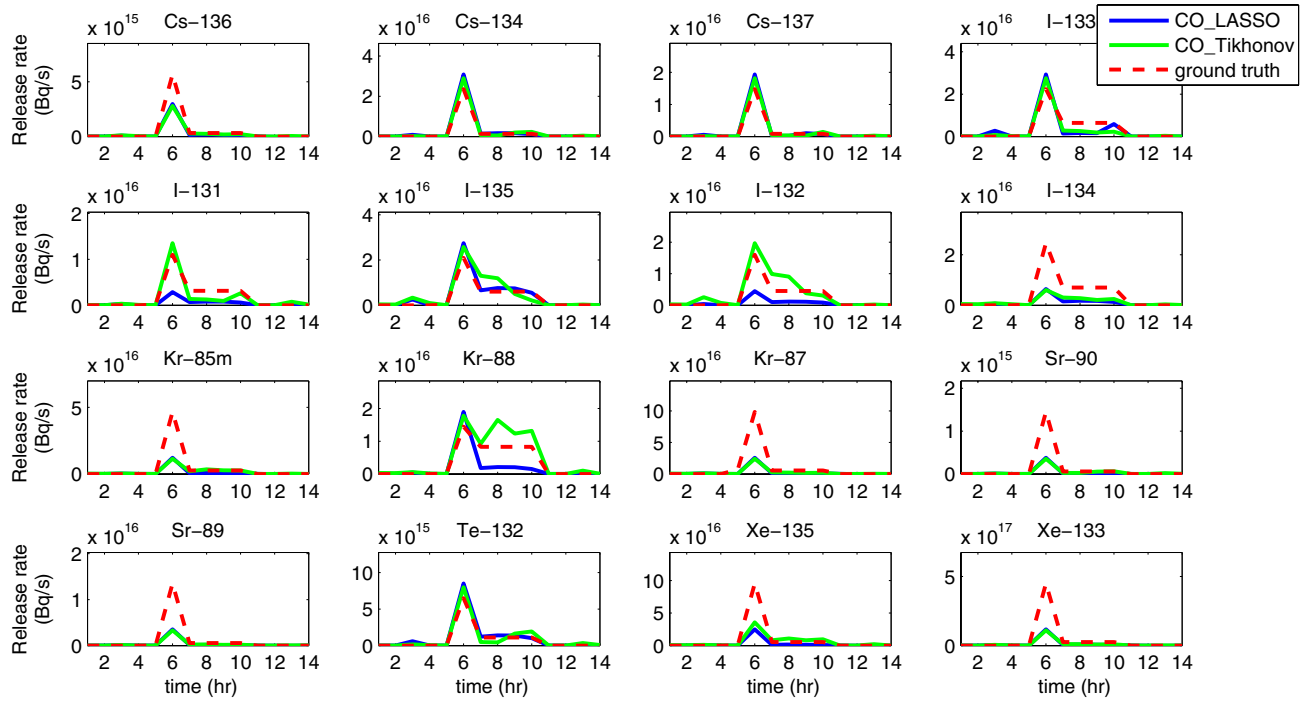

FIGURE 6 Estimated source terms using the CO_LASSO method (blue lines) and the CO_Tikhonov method (green lines) sorted by nuclides. The original source term $\mathbf{x}_{\text{true}}$ is given using dashed red lines [Colour figure can be viewed at wileyonlinelibrary.com]

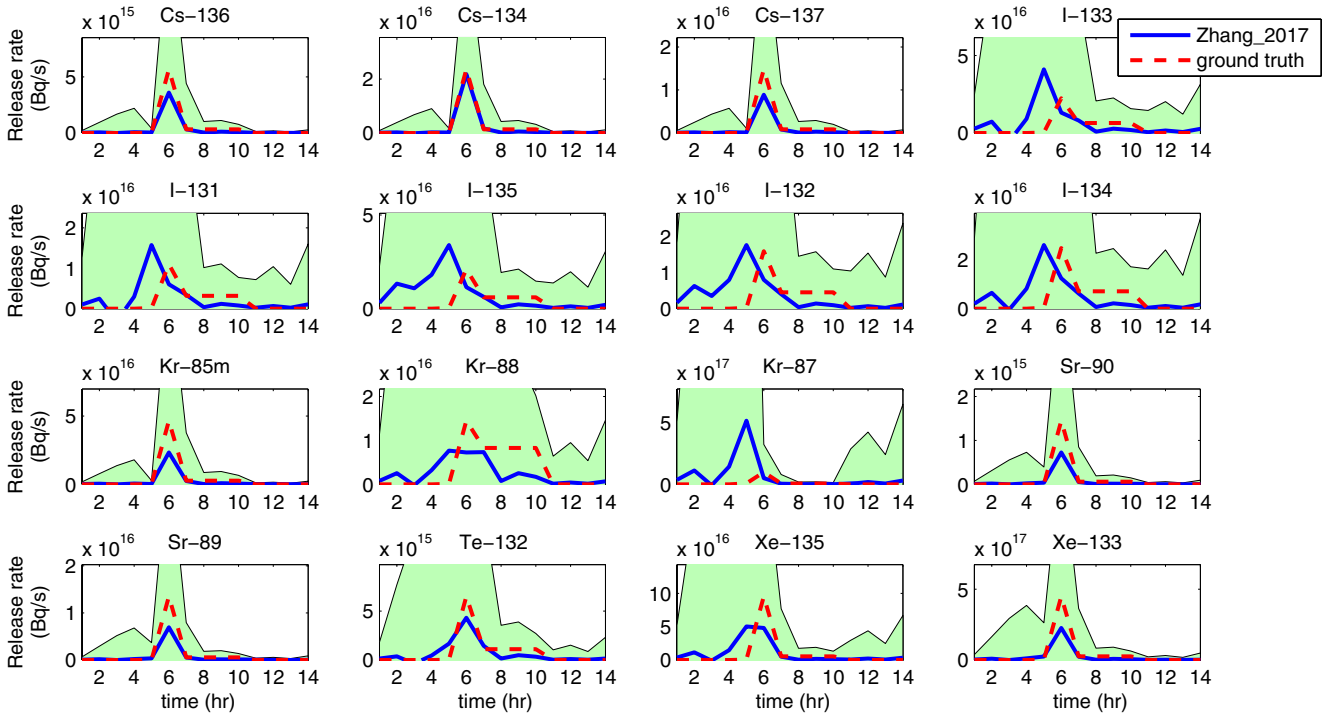

FIGURE 7 The estimated source term using the Zhang_2017 method (blue line) accompanied by the 99% highest posterior density region (green filled regions). The original source term $\mathbf{x}_{\text{true}}$ is given using dashed red lines [Colour figure can be viewed at wileyonlinelibrary.com]

of Zhang_2017. Here, the estimated source term well matches with the simulated source term. Note also that the uncertainty boundaries are tighter then in the case of Zhang_2017. In cases where the match is not estimated well, high level of uncertainty is estimated, as in the cases of Kr-88 or Sr-90. In some cases, the source term is underestimated while uncertainty boundaries are tight to estimates. The underestimation of variance is a known drawback of the variational Bayes method (Bishop, 2006), see e.g. I-135, Kr-87, or Xe-133 in Figure 8. Better results can be obtained using Monte Carlo sampling, however, at much higher computational cost.

Statistical coefficients introduced in Section 3.2 together with total estimated activities are computed for results

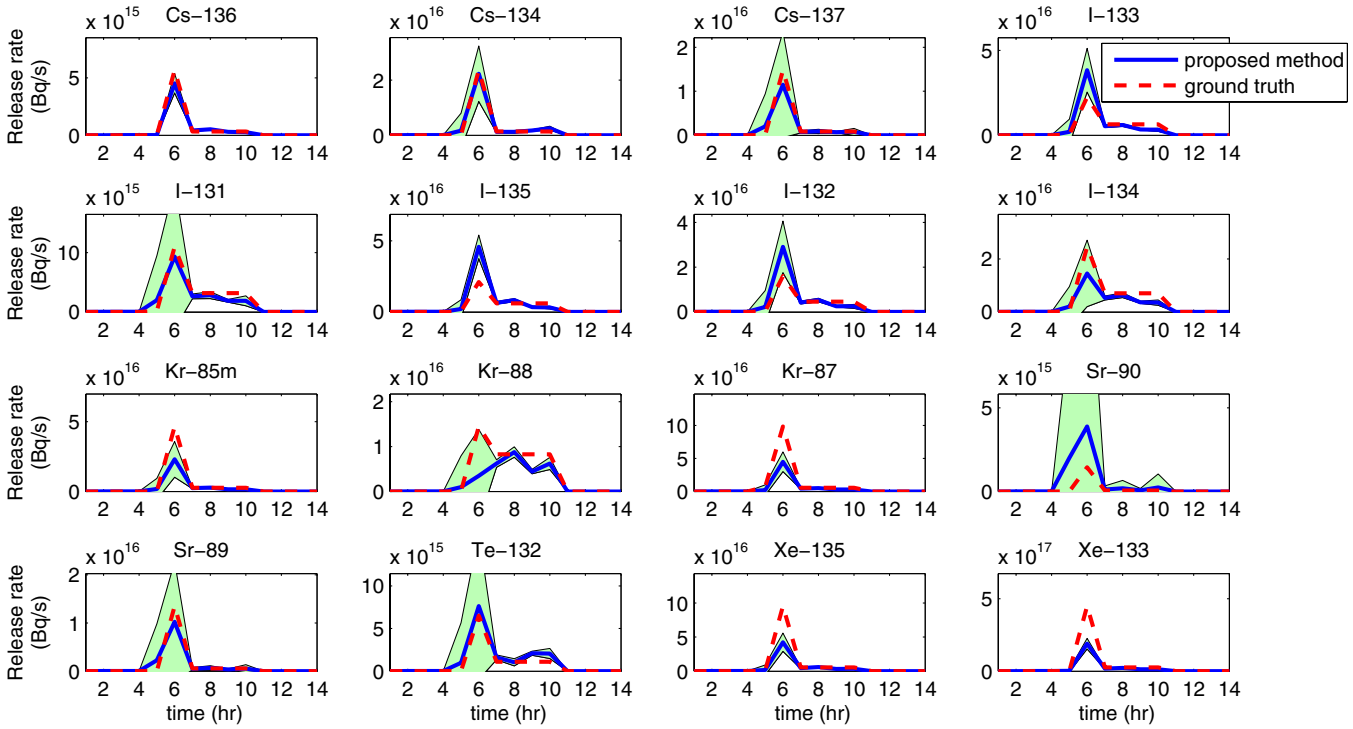

FIGURE 8 The estimated source term using the proposed method (blue line) accompanied by the 99% highest posterior density region (green filled regions). The original source term $\mathbf{x}_{\text{true}}$ is given using dashed red lines [Colour figure can be viewed at wileyonlinelibrary.com]

TABLE 2 Computed FMS, NMSE, FB, and total activity of estimated source terms from CO_LASSO and CO_Tikhonov methods, Figure 6, Zhang_2017 method, Figure 7, and the proposed method, Figure 8. Note that true total activity is 1190 PBq

	Method			
	CO_LASSO	**CO_Tikhonov**	**Zhang_2017**	**Proposed method**
FMS	0.421	0.492	0.361	0.603
NMSE	9.711	6.664	5.786	2.839
FB	0.686	0.361	−0.005	−0.092
total activity in PBq (true total is 1190 PBq)	459	638	1846	759

from the CO_LASSO and CO_Tikhonov methods, Figure 6, Zhang_2017 method, Figure 7, and the proposed method, Figure 8, and summarized in Table 2. On this example, the proposed method is comparable or outperforms all other methods based on computed statistical coefficients.

3.4 | Statistical comparison

The statistical comparison will be given for each noise level where 50 realizations of the noise on each noise level were simulated as described in detail in Section 3.1. Three statistical coefficients are computed comparing the estimated $\langle \mathbf{x} \rangle$ for each method and common $\mathbf{x}_{\text{true}}$: FMS, NMSE, and FB; and are accompanied by total estimated activities.

The results for FMS are summarized in Figure 9 using boxplots for each noise level specified in title, where red lines denote median values and blue square surrounds denote lower and upper quartiles. Note that higher value denotes better performance in the case of the FMS. The results for NMSE are summarized in Figure 10 using boxplots. The results for FB are summarized in Figure 11 where also zero level (best fit) is displayed using dashed blue lines. The total estimated mean activities are summarized in Figure 12 using boxplots while the total acitivity of the simulated source term is given using dashed lines. The results show that even relatively simple approaches such as optimization formulation with constraints and either LASSO or Tikhonov regularization terms provide reasonable results; however, with no information on uncertainty of the resulting estimates. The direct comparison between CO_LASSO and CO_Tikhonov methods suggests that the Tikhonov regularization term is more appropriate for multi-nuclide source term estimation. The Zhang_2017 method is comparable to CO_Tikhonov in terms of NMSE while it is systematically worse in terms of FMS but has great performance in terms of FB (due to the nuclide ratio means being set to true values). The performance of the proposed method is comparable with the Zhang_2017 method in terms of mean value of FB. However, it systematically outperforms all tested methods in terms of FMS and NMSE. The comparison of total estimated mean activities shows that the proposed method is more proximate to the total of simulated source term especially for more realistic noise levels 20 and 30.

In summary, the results suggest that the proposed method systematically improves the estimation of the multi-nuclide source term when constraints on nuclide ratios Equation 2 are available.

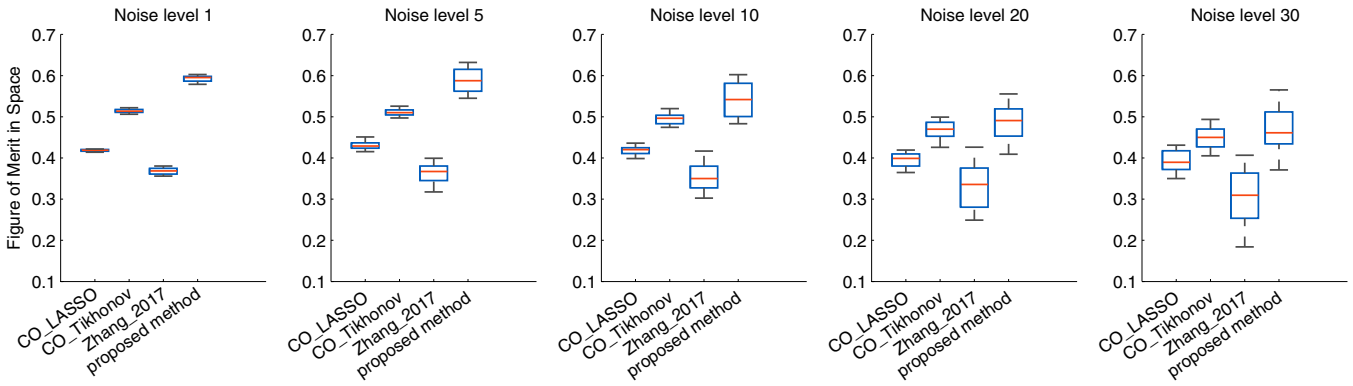

FIGURE 9 Sensitivity of the studied methods to realization of the measurement noise via boxplots of the figure of merit in space (FMS) coefficient Equation 39 – higher is better. Five noise levels with 50 realizations for each level are displayed [Colour figure can be viewed at wileyonlinelibrary.com]

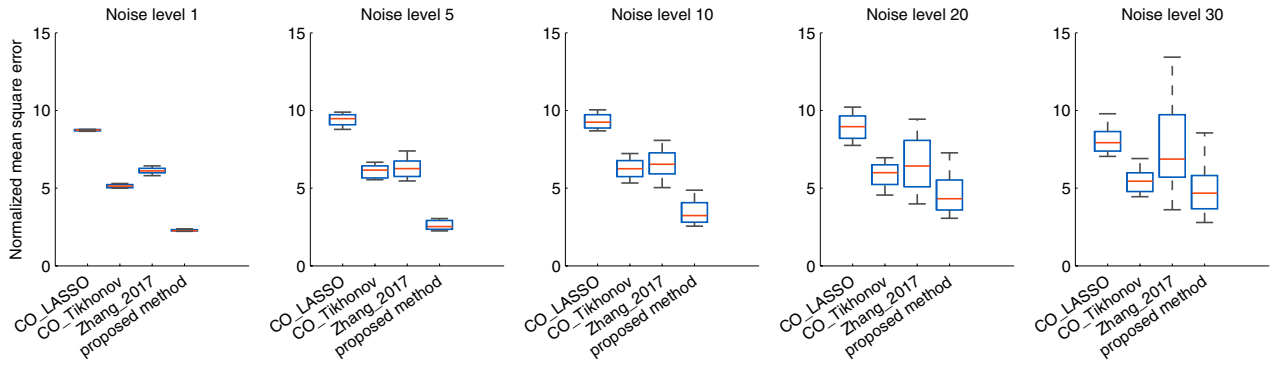

FIGURE 10 Sensitivity of the studied methods to realization of the measurement noise via boxplots of the normalized mean square error (NMSE) coefficient Equation 40 – lower is better. Five noise levels with 50 realizations for each level are displayed [Colour figure can be viewed at wileyonlinelibrary.com]

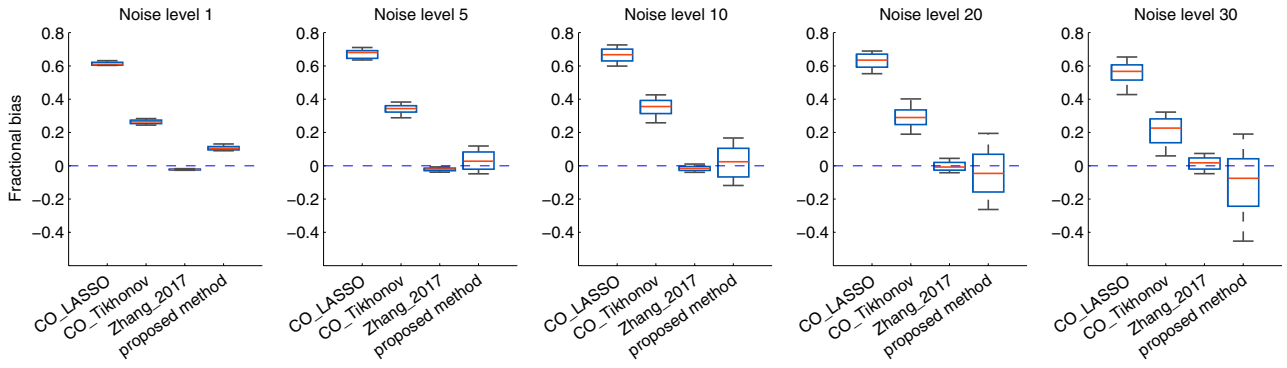

FIGURE 11 Sensitivity of the studied methods to realization of the measurement noise via boxplots of the fractional bias (FB) coefficient Equation 41 – closer to zero is better. Five noise levels with 50 realizations for each level are displayed [Colour figure can be viewed at wileyonlinelibrary.com]

4 | ESTIMATION OF CHERNOBYL CAESIUM-137 MULTI-SPECIE SOURCE TERM

In this section, the studied methods are applied to case of the Chernobyl Nuclear Power Plant (ChNPP) caesium-137 (Cs-137) source term reconstruction. For this purpose, we use the recently published dataset (Evangeliou *et al.*, 2016) that consists of 12,281 observations for Cs-137 in the form of both, deposition observations (10,682) and atmospheric concentrations (1,599). The same experimental setup (with exceptions described bellow) was used as by Evangeliou *et al.* (2017).

4.1 | Basic setup

The Lagrangian particle dispersion model FLEXPART version 10 (Stohl *et al.*, 1998; Stohl *et al.*, 2005) was used to simulate the transport and deposition of radionuclides. FLEXPART was driven by the ERA-Interim (Dee *et al.*, 2011) atmospheric reanalysis that includes four-dimensional variational analysis (4D-Var) with temporal resolution of 12 hr and spatial resolution of approximately 80 km on 60 vertical levels (from surface up to 0.1 hPa). The emissions from the ChNPP site are discretized into six vertical layers (0–0.5, 0.5–1.0, 1.0–1.5, 1.5–2.0, 2.0–2.5, 2.5–3.0 km) and 3 hr intervals from 0000 UTC on April 26, to 2100 UTC on May 5, 1986 for

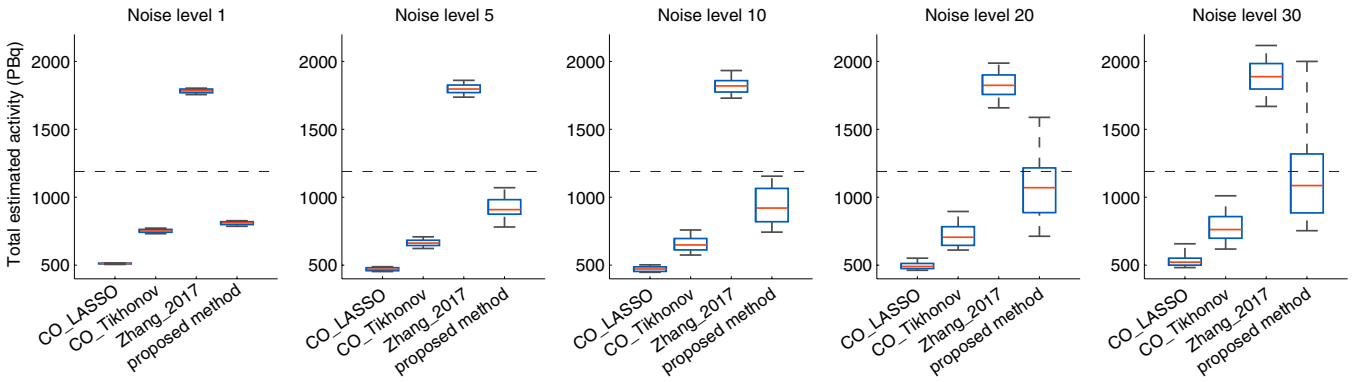

FIGURE 12 Sensitivity of the studied methods to realization of the measurement noise via boxplots of the total estimated activity. Five noise levels with 50 realizations for each level are displayed. The dashed lines denote the simulated source term with total activity of 1190 PBq [Colour figure can be viewed at wileyonlinelibrary.com]

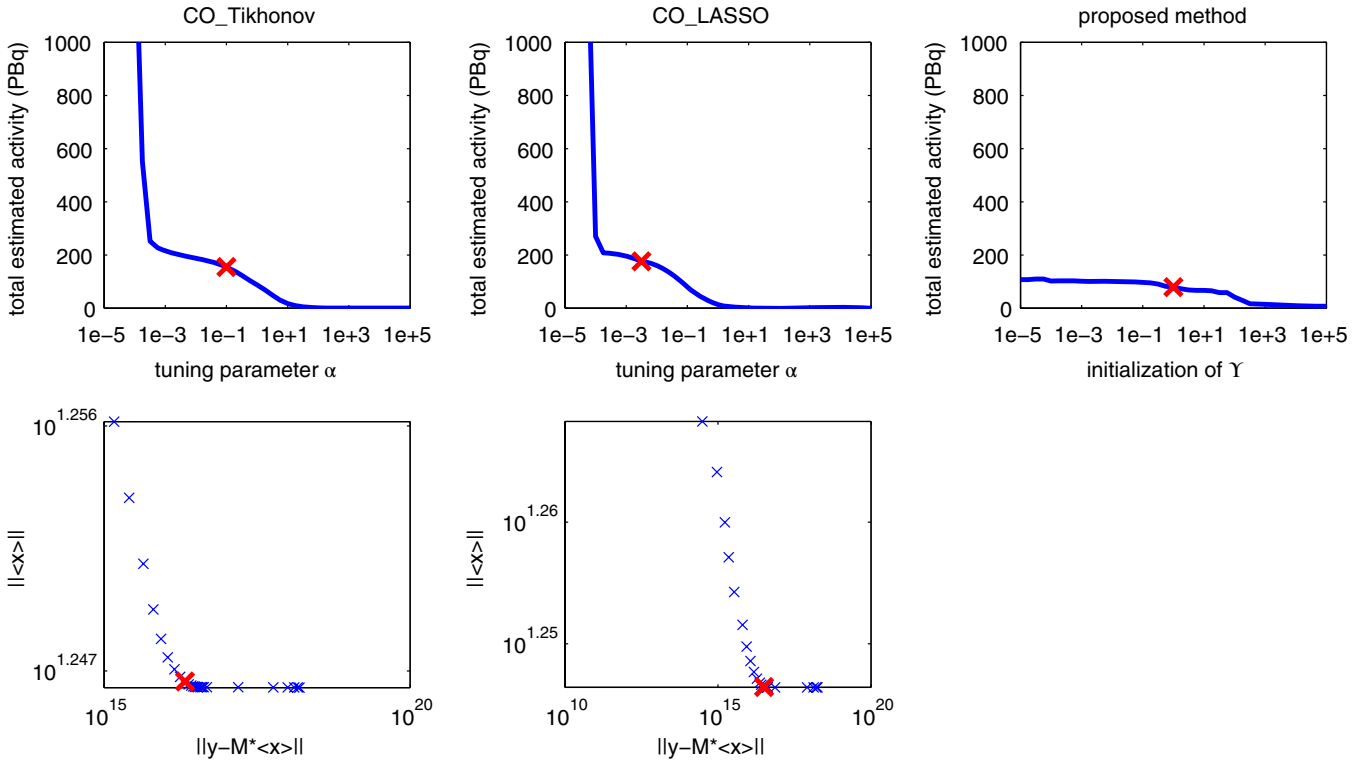

FIGURE 13 Top: total estimated activity depending on selected parameter α. Bottom: L-curves of the regularization parameters α for CO_LASSO and CO_Tikhonov methods. Red crosses denotes the selected parameter α for each method [Colour figure can be viewed at wileyonlinelibrary.com]

which the forward run of FLEXPART is done. After this time-period, it is reported that the activity declines approximately six times (De Cort *et al.*, 1998). This setup discretized the temporal-spatial domain to 480 elements for which the simulations quantify sensitivities of atmospheric activity concentrations and depositions using 300,000 particles for each release. Similarly to (Evangeliou *et al.*, 2017), we take into the account uncertainties connected with the use of deposition measurements highlighted, e.g., by Gudiksen *et al.* (1989) or Winiarek *et al.* (2014) regarded with an unknown mass of Cs-137 already deposited over Europe (mainly as a results of nuclear weapons test). However, decades after the accident, this mass has been reported (De Cort *et al.*, 1998) and already removed from the data set, see (Evangeliou *et al.*, 2017) for details. Still, this increases the uncertainty of deposition measurements. Therefore, we assume relative measurement error of 30% for concentration measurement and double (60%) for deposition measurement as suggested in (Evangeliou *et al.*, 2017). The absolute uncertainties are handled in the same way as in Stohl *et al.* (2012).

Similarly to (Evangeliou *et al.*, 2017), we assume the aerosol tracer Cs-137 subject to wet and dry deposition with four different particle sizes with aerodynamic mean diameters of 0.4, 1.2, 1.8, and 5.0 μm. Each particle is given a fixed particle size distribution that is characterised by an aerodynamic mean diameter and a logarithmic standard deviation, see Evangeliou *et al.* (2017) for details. For more information about the dry deposition scheme, we refer to (Stohl *et*

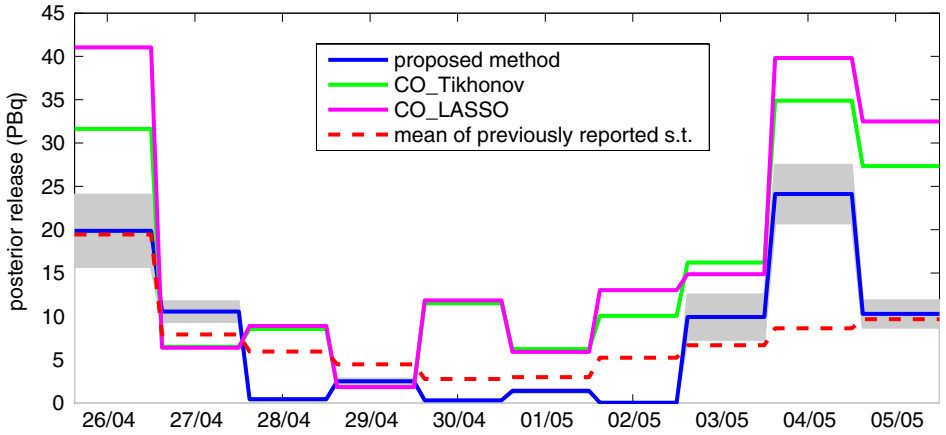

FIGURE 14 Daily estimated emissions of Cs-137 in the case of Chernobyl accident from April 26, to May 5, 1986. The mean of previously published estimates is displayed using dashed red line, the CO_Tikhonov estimate is displayed using green line, the CO_LASSO estimate is displayed using purple line, and the proposed method estimate is displayed using blue line accompanied by 95% uncertainty bounds (gray fill regions) [Colour figure can be viewed at wileyonlinelibrary.com]

al., 2005), and for the wet scavenging scheme of FLEXPART considering cloud liquid water content and cloud ice water content directly from ECMWF (European Centre for Medium-Range Weather Forecasts) fields), we refer to (Grythe *et al.*, 2017). In (Evangeliou *et al.*, 2017), it was assumed that the emitted mass is distributed as 15, 30, 40, and 15% following measured results of Malá *et al.* (2013) between the particle sizes of 0.4, 1.2, 1.8, and 5.0 μm respectively. The estimation of the source term for each fraction was calculated independently by running an inversion model using the SRS matrix for each fraction and the vector of measurements scaled by the corresponding coefficient of Malá *et al.* (2013). The fractions of these particle sizes is however unknown for new releases. Therefore, we apply the proposed methodology to the source term determination with unknown ratios of the particle sizes.

Specifically, we assume that the ratios between the first particle size and the others is known only in the form of hard bound on the ratios in the same way as in Equation 2, using bounds

$$0.3 \leq \frac{x_{k,t}}{x_{m,t}} \leq 3, \tag{42}$$

for each particle size k and each time-step $t = 1, \ldots, 80$, where the specie with particle size 0.4 μm is selected as the reference. This interval is wide enough to cover the measured ratios of the Chernobyl release which are $\frac{x_{1.2\mu m}}{x_{0.4\mu m}} = 2$, $\frac{x_{1.8\mu m}}{x_{0.4\mu m}} = 2.66$, $\frac{x_{5.0\mu m}}{x_{0.4\mu m}} = 1$ corresponding to fractions (15, 30, 40, and 15%). In our approach, the source term of all fractions is estimated from one inverse model that explains the measurements by a sum of contributions from all fractions.

Another significant difference from (Evangeliou *et al.*, 2017) is the use of the prior source term (also known as the first guess). In (Evangeliou *et al.*, 2017), the prior source term was calculated from six previously published Chernobyl source terms, (Brandt *et al.*, 2002), (Persson *et al.*, 1987), (Izrael *et al.*, 1996), (Abagyan *et al.*, 1986), (Talerko, 2005a), and from (Talerko, 2005b), as their mean emission estimate, and then used in inversion scheme. In the proposed method, we do not assume any prior information on the source term other than the ratios. Therefore, we will not use previous estimates in any way. They will serve only for validation of the obtained results.

4.2 | Results

Here, we summarize and discuss the results of the studied methods. Note that only results from the CO_Tikhonov, CO_LASSO, and the proposed method are available since the method Zhang_2017 assumes data in specific format and time discretization which is not compatible with the studied Chernobyl case.

The inversion setup for Chernobyl Cs-137 source term is non-standard in a way that we have six different vertical layers with four different particle sizes. Hence, we calculate the source term for each vertical layer separately with four parts of the source term related to each specie with different particle size. This results in an estimated source term (10 days with temporal resolution of 3 hr) for each vertical layer and each specie, which can be summed up to obtain the overall source term for each method.

Similarly as in the previous twin experiment, the CO_LASSO and CO_Tikhonov methods need to preselect the regularization parameter α. Therefore, we calculate the L-curves (Hansen, 1992) for each method as displayed in Figure 13. There are calculated total estimated activities depending on selected α (top row) and L-curves (bottom row). We selected the regularization parameter α as follows: $\alpha_{\text{LASSO}} = 10^{-2.5}$ and $\alpha_{\text{Tikhonov}} = 10^{-1}$. As can be seen from Figure 13, the sensitivity on selection of the regularization parameter is relatively high. The proposed method may also yield different results when initialized from different starting point. We have identified that the most sensitive initialization parameter in is the initial value $\boldsymbol{\Upsilon}_{\text{init}} = \alpha_{\text{init}}\mathbf{I}_n$. The sensitivity of the results to this choice is also displayed in Figure 13,

TABLE 3 Summarized fractions of particle sizes in the estimated source terms accompanied by the total estimated activity. The fraction values in the bottom line of the table are experimentally obtained results of Malá *et al.* (2013)

Method	F_1 (%)	F_2 (%)	F_3 (%)	F_4 (%)	Total estimated activity (PBq)
CO_LASSO	22	22	24	32	176
CO_Tikhonov	21	24	23	32	155
Proposed method	13	33	35	19	79 ± 14
Mean of previously published source terms	15	30	40	15	74 ± 15

top right. In the case of the proposed method, the default selection is $\alpha_{\text{init}} = 1$ yielding $\boldsymbol{\Upsilon}_{\text{init}} = \mathbf{I}_n$.

The estimated daily posterior emissions are displayed in Figure 14 associated with the total estimated activity in Table 3. The consensus of previously reported values is displayed as dashed red line in Figure 14 with a total of 74 ± 15 PBq and will be used for comparison with our results.

The CO_LASSO method (purple line in Figure 14) estimated the total activity of 176 PBq which is more then twice higher then the consensus with high Cs-137 emissions especially in the first day and in the ninth day of the Chernobyl accident. The CO_Tikhonov method (green line in Figure 14) estimated the total activity of 155 PBq with estimated activity approximately twice higher then the consensus Cs-137 total emission. Note that temporal profiles from the CO_LASSO and CO_Tikhonov methods are similar in the middle of the studied period while CO_LASSO estimates are higher in the beginning and at the end of the studied period. The proposed method (blue line with 95% uncertainty bounds using gray color in Figure 14) estimated the total activity of 79 ± 14 PBq which is in agreement with the consensus as well as with recently published results by (Liu *et al.*, 2017) with range 70–130 PBq and with results by Evangeliou *et al.* (2017) with estimated total emission 86 ± 5 PBq. The source term was underestimated in the middle of the 10-day period and overestimated at the end of the studied period.

The fraction of the particle sizes that were assumed to be approximately known from Malá *et al.* (2013) were calculated from the results of the estimation methods as follows

$$F_i = \frac{||\mathbf{x}_i||_1}{\sum_i ||\mathbf{x}_i||_1}. \tag{43}$$

The results are displayed in Table 3. Interestingly, the fractions computed from posterior estimates of the proposed method are in good agreement with the measured results of Malá *et al.* (2013) which are given in brackets bellow. Estimated percentage of the proposed method for emitted mass for particle size of 0.4 μm is 13% (15%), for 1.2 μm is 33% (30%), for 1.8 μm is 35% (40%), and for 5.0 μm is 19% (15%). Note that such agreement is not obtained neither by CO_Tikhonov method nor CO_LASSO method, see Table 3.

Figure 15 shows the scatter plots of measurements $\mathbf{y}$ and reconstructions $\mathbf{M}\langle\mathbf{x}\rangle$. Note that on the level of $\mathbf{y} \approx 10^{-1}$ source terms from all methods (including the consensus source term) yield estimates significantly lower than the measurement. The predicted values using source term from the proposed method are closer to the ideal correspondence than others.

5 | CONCLUSION

The problem of multi-species source term reconstruction from unspecific measurements is studied in two special cases: estimation of multi-nuclide source term from the gamma dose rate (GDR) measurements and estimation of the single nuclide source term composed of different particle sizes. Since the problem itself is ill-conditioned, similarly to Saunier *et al.* (2013) we assume approximate knowledge on ratio of the species as a prior information about the problem. We proposed a Bayesian formulation of problem where a prior bounds on the specie ratios are used to restrict the covariance matrix of the source term using prior distributions on elements of the covariance matrix. All other parameters of the proposed model have their own prior distributions and are estimated within the model. We propose an estimation procedure using the variational Bayes method that leads to an iterative algorithm which is publicly available for download.

The proposed method is evaluated and compared with state-of-the-art methods on a twin experiment of a release

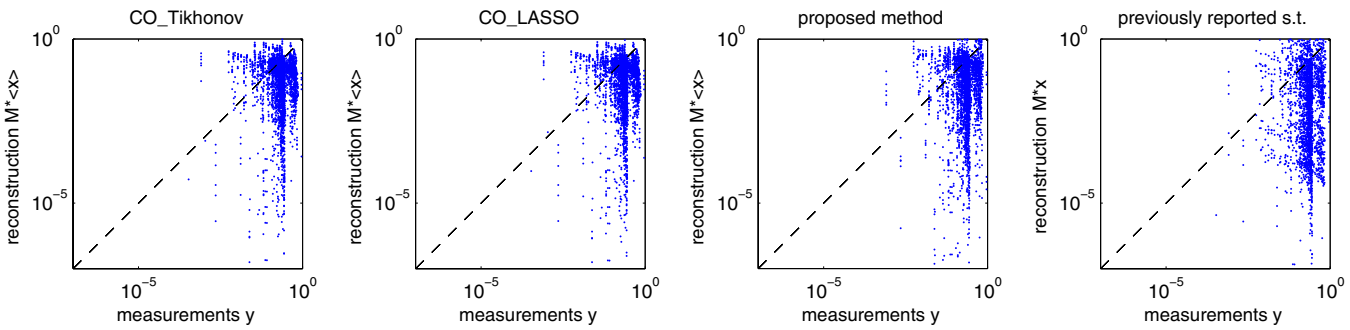

FIGURE 15 Scatter plots between measurements and reconstructions for each tested method and for mean of previously reported estimates [Colour figure can be viewed at wileyonlinelibrary.com]

consisting of 16 nuclides from the Czech nuclear power Temelin, while response on the Austrian GDR measurement network is considered. We have shown that the proposed method outperforms other state-of-the-art methods under different noise conditions without the necessity of manual tuning. The proposed method could also be used for sequential estimation on receding window and thus used for continuous monitoring and assessment evaluation.

The method is validated on the problem of estimation of the caesium-137 source term from the Chernobyl accidental release (Evangeliou *et al.*, 2016), where the source term is composed from four species differing in particle sizes. We have set the prior range on the ratios of the species and estimated them jointly with the source term. The total emission estimated using the proposed method, 79 ± 14 PBq, is in agreement with previously reported total emission rates. Moreover, the estimated fractions of the particle sizes were 13% for 0.4 μm, 33% for 1.2 μm, 35% for 1.8 μm, and 19% for 5.0 μm which is in agreement with measured results of Malá *et al.* (2013) with fractions 15, 35, 40, and 15% respectively.

ACKNOWLEDGEMENTS

This research was supported by EEA/Norwegian Financial Mechanism under project MSMT-28477/2014 Source-Term Determination of Radionuclide Releases by Inverse Atmospheric Dispersion Modelling (STRADI). We would like to thank to the editor of this paper as well as to two anonymous reviewers for valuable comments.

REFERENCES

Abagyan, A., Ilyin, L., Izrael, Y., Legasov, V. and Petrov, V. (1986) The information on the Chernobyl accident and its consequences, prepared for IAEA. *Sov. At. Energy*, 61, 301–320. https://doi.org/10.1007/BF01122262.

Abida, R. and Bocquet, M. (2009) Targeting of observations for accidental atmospheric release monitoring. *Atmospheric Environment*, 43(40), 6312–6327.

Aliyu, A., Evangeliou, N., Mousseau, T., Wu, J. and Ramli, A. (2015) An overview of current knowledge concerning the health and environmental consequences of the Fukushima Daiichi nuclear power plant (FDNPP) accident. *Environment international*, 85, 213–228.

Bishop, C. (2006) *Pattern recognition and machine learning*. Springer.

Bocquet, M. (2005) Reconstruction of an atmospheric tracer source using the principle of maximum entropy. *I: Theory, Quarterly Journal of the Royal Meteorological Society*, 131(610), 2191–2208.

Bocquet, M. (2007) High-resolution reconstruction of a tracer dispersion event: application to ETEX. *Quarterly Journal of the Royal Meteorological Society*, 133(625), 1013–1026.

Bocquet, M. (2008) Inverse modelling of atmospheric tracers: non-gaussian methods and second-order sensitivity analysis. *Nonlinear Processes in Geophysics*, 15(1), 127–143.

Brandt, J., Christensen, J. and Frohn, L. (2002) Modelling transport and deposition of caesium and iodine from the Chernobyl accident using the DREAM model. *Atmospheric Chemistry and Physics*, 2(5), 397–417.

Chang, J. and Hanna, S. (2004) Air quality model performance evaluation. *Meteorology and Atmospheric Physics*, 87(1), 167–196.

Davoine, X. and Bocquet, M. (2007) Inverse modelling-based reconstruction of the Chernobyl source term available for long-range transport. *Atmospheric Chemistry and Physics*, 7(6), 1549–1564.

De Cort, M., Dubois, G., Fridman, S., Germenchuk, M., Izrael, Y., Janssens, A., Jones, A., Kelly, G., Kvasnikova, E., Matveenko, I., Nazarov, I., Pokumeiko, Y., Sitak, V., Stukin, E., Tabachny, L., Tsaturov, Y. and Avdyushin, S. (1998) *Atlas of caesium deposition on europe after the Chernobyl accident* pp. 1–63. EU - Office for Official Publications of the European Communities.

Dee, D., Uppala, S., Simmons, A., Berrisford, P., Poli, P., Kobayashi, S., Andrae, U., Balmaseda, M., Balsamo, G., Bauer, P., Bechtold, P., Beljaars, A., van de Berg, L., Bidlot, J., Bormann, N., Delsol, C., Dragani, R., Fuentes, M., Geer, A., Haimberger, L., Healy, S., Hersbach, H., Hólm, E., Isaksen, L., Kallberg, P., Kohler, M., Matricardi, M., Mcnally, A., Monge-Sanz, B., Morcrette, J., Park, B., Peubey, C., de Rosnay, P., Tavolato, C., Thepaut, J. and Vitart, F. (2011) The ERA-interim reanalysis: configuration and performance of the data assimilation system. *Quarterly Journal of the royal meteorological society*, 137(656), 553–597.

Eckhardt, S., Prata, A., Seibert, P., Stebel, K. and Stohl, A. (2008) Estimation of the vertical profile of sulfur dioxide injection into the atmosphere by a volcanic eruption using satellite column measurements and inverse transport modeling. *Atmospheric Chemistry and Physics*, 8(14), 3881–3897.

Evangeliou, N., Hamburger, T., Cozic, A., Balkanski, Y. and Stohl, A. (2017) Inverse modeling of the Chernobyl source term using atmospheric concentration and deposition measurements. *Atmospheric Chemistry and Physics*, 17(14), 8805–8824.

Evangeliou, N., Hamburger, T., Talerko, N., Zibtsev, S., Bondar, Y., Stohl, A., Balkanski, Y., Mousseau, T. and Møller, A. (2016) Reconstructing the Chernobyl nuclear power plant (CNPP) accident 30 years after. *A unique database of air concentration and deposition measurements over Europe, Environmental pollution*, 216, 408–418.

Golub, G., Hansen, P. and O'Leary, D. (1999) Tikhonov regularization and total least squares. *SIAM Journal on Matrix Analysis and Applications*, 21(1), 185–194.

Grant, M., Boyd, S., Blondel, V., Boyd, S., Kimura, H. and (eds) (2008) Graph implementations for nonsmooth convex programs *Recent Advances in Learning and Control*. Springer-Verlag Limited: Lecture Notes in Control and Information Sciences, pp. 95–110.

Grant, M. and Boyd, S. (2014) *CVX: Matlab software for disciplined convex programming*. version 2.1. http://cvxr.com/cvx.

Grythe, H., Kristiansen, N., Zwaaftink, C., Eckhardt, S., Ström, J., Tunved, P., Krejci, R. and Stohl, A. (2017) A new aerosol wet removal scheme for the lagrangian particle model flexpart. *Geoscientific Model Development*, 10(4), 1447–1466.

Gudiksen, P.H., Harvey, T.F. and Lange, R. (1989) Chernobyl source term, atmospheric dispersion, and dose estimation. *Health Physics*, 57(5), 697–706.

Hansen, P. (1992) Analysis of discrete ill-posed problems by means of the L-curve. *SIAM review*, 34(4), 561–580.

Hofman, R., Seibert, P., Kovalets, I. and Andronopoulos, S. (2015) Analytical source term optimization for radioactive releases with approximate knowledge of nuclide ratios, EGU General Assembly Conference Abstracts. *Vol.*, 17, 3033.

Issartel, J.-P. and Baverel, J. (2003) Inverse transport for the verification of the comprehensive nuclear test ban treaty. *Atmospheric Chemistry and Physics*, 3(3), 475–486.

Izrael, Y., De Cort, M., Jones, A., Nazarov, I., Fridman, S., Kvasnikova, E., Stukin, E., Kelly, G., Matveenko, I., Pokumeiko, Y., Tabatchnyi, L. and Tsaturon, Y. (1996) *The Atlas of Caesium-137 Contamination of Europe after the Chernobyl Accident*. Minsk, Belarus: The Radiological Consequences of the Chernobyl Accident. Proceedings of the First International Conference.

Joint working group of Radiation Protection Bureau, H.e.a.l.t.h.C.a.n.a.d.a., Atomic Energy Control Board (1999) *Recommendations on Dose Coefficients for Assessing Doses from Accidental Radionuclide Releases to the Environment*. Health Canada: Ottawa - Ontario.

Jordan, M., Ghahramani, Z., Jaakkola, T. and Saul, L. (1999) An introduction to variational methods for graphical models. *Machine learning*, 37(2), 183–233.

Katata, G., Ota, M., Terada, H., Chino, M. and Nagai, H. (2012) Atmospheric discharge and dispersion of radionuclides during the Fukushima Dai-ichi nuclear power plant accident. *Part I: Source term estimation and local-scale atmospheric dispersion in early phase of the accident, Journal of Environmental Radioactivity*, 109, 103–113.

Kovalets, I., Andronopoulos, S., Hofman, R., Seibert, P. and Ievdin, I. (2016) *Advanced Method for Source Term Estimation and Status of its Integration in JRODOS*, Vol. 51(HS 2) pp. S121–S123.

Kovalets, I., Hofman, R., Seibert, P., Andronopoulos, S. and Ievdin, I. (2016) *Description of software module for source term estimation using advanced method integrated in DSS RODOS*. report of the EC FP7 PREPARE project PREPARE(WP4)-(16)-04. Available at:. https://doi.org/10.13140/RG.2.1.5169.1285.

Kristiansen, N., Stohl, A., Prata, A., Richter, A., Eckhardt, S., Seibert, P., Hoffmann, A., Ritter, C., Bitar, L., Duck, T. and Stebel, K. (2010) Remote sensing and inverse Transport Modeling of the Kasatochi Eruption Sulfur Dioxide Cloud, 115(D2), 1984–2012.

Kuča, P., Prouza, Z., Češprová, I., Marešová, B. and Pecha P., H.R. (2012) *Modelling the impact of a hypothetical release of radionuclides from a nuclear facility applications este a harp* p. 44. (in czech) Available at:. http://www.utia.cz/node/631/0384897.

Kullback, S. and Leibler, R. (1951) On information and sufficiency. *Annals of Mathematical Statistics*, 22(1), 79–86.

Leelössy, Á., Lagzi, I., Kovács, A. and Mészáros, R. (2018) A review of numerical models to predict the atmospheric dispersion of radionuclides. *Journal of environmental radioactivity*, 182, 20–33.

Leelössy, Á., Mészáros, R., Kovács A, Lagzi, I. and Kovács, T. (2017) Numerical simulations of atmospheric dispersion of iodine-131 by different models. *PloS one*, 12(e0172312).

Liu, Y., Haussaire, J.-M., Bocquet, M., Roustan, Y., Saunier, O. and Mathieu, A. (2017) Uncertainty quantification of pollutant source retrieval: comparison of Bayesian methods with application to the Chernobyl and Fukushima Daiichi accidental releases of radionuclides. *Quarterly Journal of the Royal Meteorological Society*, 143(708), 2886–2901.

Malá, H., Rulk, P., Bečková, V., Mihalk, J. and Slezáková, M. (2013) Particle size distribution of radioactive aerosols after the Fukushima and the Chernobyl accidents. *Journal of Environmental Radioactivity*, 126, 92–98.

Nisbet, E. and Weiss, R. (2010) Top-down versus bottom-up. *Science*, 328(5983), 1241–1243.

Persson, C., Rodhe, H. and De Geer, L.-E. (1987) The Chernobyl accident: a meteorological analysis of how radionuclides reached and were deposited in Sweden. *Ambio*, 16(1), 20–31.

Rajaona, H., Septier, F., Armand, P., Delignon, Y., Olry, C., Albergel, A. and Moussafir, J. (2015) An adaptive Bayesian inference algorithm to estimate the parameters of a hazardous atmospheric release. *Atmospheric Environment*, 122, 748–762.

Saunier, O., Mathieu, A., Didier, D., Tombette, M., Quélo, D., Winiarek, V. and Bocquet, M. (2013) An inverse modeling method to assess the source term of the Fukushima nuclear power plant accident using gamma dose rate observations. *Atmospheric Chemistry and Physics*, 13(22), 11403–11421.

Savushkin, I., Ravkova, E., Gourko, O. and Ulanovskij, A. (1998) *Construction of a set of typical VVER-1000 severe accident source terms for training applications of RODOS*. Institute of Power Engineering Problems, Minsk. RODOS(WG7)-TN(98)1.

Seibert, P. (2000) Inverse modelling of sulfur emissions in europe based on trajectories. *Inverse Methods in Global Biogeochemical Cycles*, 147–154.

Seibert, P. and Frank, A. (2004) Source-receptor matrix calculation with a Lagrangian particle dispersion model in backward mode. *Atmospheric Chemistry and Physics*, 4(1), 51–63.

Šmídl, V. and Hofman, R. (2014) Efficient sequential Monte Carlo sampling for continuous monitoring of a radiation situation. *Technometrics*, 56(4), 514–528.

Šmídl, V. and Quinn, A. (2006) *The Variational Bayes Method in Signal Processing*. Springer.

Stohl, A., Forster, C., Frank, A., Seibert, P. and Wotawa, G. (2005) Technical note: the Lagrangian particle dispersion model FLEXPART version 6.2. *Atmospheric Chemistry and Physics*, 5(9), 2461–2474.

Stohl, A., Hittenberger, M. and Wotawa, G. (1998) Validation of the lagrangian particle dispersion model flexpart against large-scale tracer experiment data. *Atmospheric Environment*, 32(24), 4245–4264.

Stohl, A., Prata, A., Eckhardt, S., Clarisse, L., Durant, A., Henne, S., Kristiansen, N., Minikin, A., Schumann, U., Seibert, P., Stebel, K., Thomas, H.E., Thorsteinsson, T., Tørseth, K. and Weinzierl, B. (2011) Determination of time-and height-resolved volcanic ash emissions and their use for quantitative ash dispersion modeling: the 2010 eyjafjallajökull eruption. *Atmospheric Chemistry and Physics*, 11(9), 4333–4351.

Stohl, A., Seibert, P., Wotawa, G., Arnold, D., Burkhart, J., Eckhardt, S., Tapia, C., Vargas, A. and Yasunari, T. (2012) Xenon-133 and caesium-137 releases into the atmosphere from the Fukushima dai-ichi nuclear power plant: determination of the source term, atmospheric dispersion, and deposition. *Atmospheric Chemistry and Physics*, 12(5), 2313–2343.

Talerko, N. (2005a) Mesoscale modelling of radioactive contamination formation in Ukraine caused by the Chernobyl accident. *Journal of environmental radioactivity*, 78(3), 311–329.

Talerko, N. (2005b) Reconstruction of 131i radioactive contamination in Ukraine caused by the Chernobyl accident using atmospheric transport modelling. *Journal of environmental radioactivity*, 84(3), 343–362.

Thompson, I., Andersen, C., Bøtter-Jensen, L., Funck, E., Neumaier, S. and Sáez-Vergara, J. (2000) An international intercomparison of national network systems used to provide early warning of a nuclear accident having transboundary implications. *Radiation protection dosimetry*, 92(1–3), 89–100.

Tibshirani, R. (1996) Regression shrinkage and selection via the lasso. *Journal of the Royal Statistical Society. Series B (Methodological)*, 58(1), 267–288.

Tichý, O., Šmídl, V., Hofman, R. and Stohl, A. (2016) LS-APC v1.0: a tuning-free method for the linear inverse problem and its application to source-term determination. *Geoscientific Model Development*, 9(11), 4297–4311.

Tichý, O., Šmídl, V., Hofman, R., Šindelářová, K., Hýža, M. and Stohl, A. (2017) Bayesian inverse modeling and source location of an unintended ^{131}I release in Europe in the fall of 2011. *Atmospheric Chemistry and Physics*, 17(20), 12677–12696.

Winiarek, V., Bocquet, M., Duhanyan, N., Roustan, Y., Saunier, O. and Mathieu, A. (2014) Estimation of the caesium-137 source term from the Fukushima Daiichi nuclear power plant using a consistent joint assimilation of air concentration and deposition observations. *Atmospheric environment*, 82, 268–279.

Winiarek, V., Bocquet, M., Saunier, O. and Mathieu, A. (2012) Estimation of errors in the inverse modeling of accidental release of atmospheric pollutant: application to the reconstruction of the cesium-137 and iodine-131 source terms from the Fukushima Daiichi power plant. *Journal of Geophysical Research: Atmospheres*, 117, D05122.

Winiarek, V., Vira, J., Bocquet, M., Sofiev, M. and Saunier, O. (2011) Towards the operational estimation of a radiological plume using data assimilation after a radiological accidental atmospheric release. *Atmospheric environment*, 45(17), 2944–2955.

Zhang, X., Raskob, W., Landman, C., Trybushnyi, D., Haller, C. and Yuan, H. (2017) Automatic plume episode identification and cloud shine reconstruction method for ambient gamma dose rates during nuclear accidents. *Journal of Environmental Radioactivity*, 178, 36–47.

Zhang, X., Raskob, W., Landman, C., Trybushnyi, D. and Li, Y. (2017) Sequential multi-nuclide emission rate estimation method based on gamma dose rate measurement for nuclear emergency management. *Journal of Hazardous Materials*, 325, 288–300.

Zhang, X., Su, G., Chen, J., Raskob, W., Yuan, H. and Huang, Q. (2015) Iterative ensemble Kalman filter for atmospheric dispersion in nuclear accidents: an application to Kincaid tracer experiment. *Journal of hazardous materials*, 297, 329–339.

How to cite this article: Tichý O, Šmídl V, Hofman R, Evangeliou N. Source term estimation of multi-specie atmospheric release of radiation from gamma dose rates. *Q J R Meteorol Soc.* 2018;1–17. https://doi.org/10.1002/qj.3403

APPENDIX: TRUNCATED GAUSSIAN DISTRIBUTION

Truncated Gaussian distribution, denoted as $\mathcal{N}^{\text{tr}}$, of a scalar variable x on interval $[a;b]$ is defined as

$$\mathcal{N}^{\text{tr}}(\mu,\sigma,[a,b]) = \frac{\sqrt{2}\exp\left(-\frac{1}{2\sigma}(x-\mu)^2\right)}{\sqrt{\pi\sigma}(erf(\beta)-erf(\alpha))}\chi_{[a,b]}(x), \quad (44)$$

where $\alpha = \frac{a-\mu}{\sqrt{2\sigma}}$, $\beta = \frac{b-\mu}{\sqrt{2\sigma}}$, function $\chi_{[a,b]}(x)$ is a characteristic function of interval $[a,b]$ defined as $\chi_{[a,b]}(x) = 1$ if $x \in [a,b]$ and $\chi_{[a,b]}(x) = 0$ otherwise. erf() is the error function defined as $\text{erf}(t) = \frac{2}{\sqrt{\pi}}\int_0^t e^{-u^2}\text{d}u$.

The moments of truncated Gaussian distribution are

$$\langle x\rangle = \mu - \sqrt{\sigma}\frac{\sqrt{2}[\exp(-\beta^2) - \exp(-\alpha^2)]}{\sqrt{\pi}(\mathrm{erf}(\beta) - \mathrm{erf}(\alpha))}, \tag{45}$$

$$\left\langle x^2\right\rangle = \sigma + \mu\hat{x} - \sqrt{\sigma}\frac{\sqrt{2}[b\exp(-\beta^2) - a\exp(-\alpha^2)]}{\sqrt{\pi}(\mathrm{erf}(\beta) - \mathrm{erf}(\alpha))}. \tag{46}$$

Multivariate truncated Gaussian distribution

Truncation of the multivariate Normal distribution of the vector $\mathbf{x}$, $\mathbf{x} \sim \mathcal{N}^{\mathrm{tr}}(\boldsymbol{\mu}, \Sigma_{\mathbf{x}}, [a, b])$, is formally simple, however, analytically intractable. Hence, we approximate the moments of the vector $\mathbf{x}$ of the truncated Normal distribution using moments of

$$\tilde{\mathbf{x}} \sim \mathcal{N}^{\mathrm{tr}}(\boldsymbol{\mu}, \mathrm{diag}(\boldsymbol{\sigma}_{\mathbf{x}}), [a, b]), \tag{47}$$

where $\boldsymbol{\sigma}_{\mathbf{x}}$ is a vector of diagonal elements of $\Sigma_{\mathbf{x}}$ corresponding to the approximation of the posterior by a product of marginals Equation 44 with mean value $\langle\mathbf{x}\rangle$ with elements given by Equation 45 and $\left\langle\mathbf{x}\mathbf{x}^T\right\rangle = \langle\mathbf{x}\rangle\langle\mathbf{x}\rangle^T + \mathrm{diag}(\langle\boldsymbol{\sigma}\rangle)$, where $\langle\sigma\rangle_i = \left\langle x_i^2\right\rangle - \langle x\rangle_i^2$. However, it may be too coarse approximation since it ignores covariance of the elements. An alternative is to approximate

$$\left\langle\mathbf{x}\mathbf{x}^T\right\rangle = \langle\mathbf{x}\rangle\langle\mathbf{x}\rangle^T + \mathrm{diag}(\mathbf{o})\Sigma_{\mathbf{x}}\mathrm{diag}(\mathbf{o}), \tag{48}$$

where $\mathbf{o}$ is a vector of elements $o_i = \langle\sigma\rangle_i^{1/2}\sigma_i^{-1/2}$. Heuristics Equation 48 is motivated by the observation that for a Normal distribution with the main mass far from the truncation lines, $o_i \to 1$ and Equation 48 becomes equivalent to the moment of the non-truncated Normal distribution.

SHAPING PARAMETERS OF POSTERIOR DISTRIBUTIONS

The shaping parameters of the posterior distributions Equations 24–30 as follows:

$$\Sigma_{\mathbf{x}} = \left(\langle\omega\rangle\mathbf{M}^T\mathbf{M} + \left\langle\mathbf{L}\Upsilon\mathbf{L}^T\right\rangle\right)^{-1}, \tag{49}$$

$$\mu_{\mathbf{x}} = \Sigma_{\mathbf{x}}\left(\langle\omega\rangle\mathbf{M}^T\mathbf{y}\right), \tag{50}$$

$$\boldsymbol{\alpha} = \alpha_0 + \frac{1}{2}\mathbf{1}_{q,1}, \tag{51}$$

$$\boldsymbol{\beta} = \beta_0 + \frac{1}{2}\mathrm{diag}\Big(\left\langle\mathbf{L}_m^T\mathbf{x}_m\mathbf{x}_m^T\mathbf{L}_m\right\rangle + \tag{52}$$

$$+ \frac{1}{\delta}\sum_{k=1}^{(m-1)}\left\langle\mathbf{L}_k^T\mathbf{x}_k\mathbf{x}_k^T\mathbf{L}_k\right\rangle\Big), \tag{53}$$

$$\Sigma_{l_{m,t}} = \Big(\left\langle\upsilon_{q(m-1)+t}\right\rangle\left\langle x_{q(m-1)+t}x_{q(m-1)+t}\right\rangle + \tag{54}$$

$$+ \mathrm{diag}(\langle\psi_{m,t}\rangle)\Big)^{-1}, \tag{55}$$

$$\mu_{l_{m,t}} = \Sigma_{l_{m,t}}\Big(\left\langle x_{q(m-1)+t+1}x_{q(m-1)+t}\right\rangle\times \tag{56}$$

$$\times\left\langle\upsilon_{q(m-1)+t}\right\rangle + l_0\mathrm{diag}(\langle\psi_{m,t}\rangle)\Big), \tag{57}$$

$$\zeta_{m,t} = \zeta_0 + \frac{1}{2},\ t = 1, \ldots, q-1, \tag{58}$$

$$\eta_{m,t} = \eta_0 + \frac{1}{2}\left\langle l_{m,t}^2\right\rangle - l_0\langle l_{m,t}\rangle + \frac{1}{2}l_0^2, \tag{59}$$

$$\Sigma_{l_{k,t}} = \Big(\left\langle\upsilon_{q(k-1)+t}\right\rangle\left\langle x_{q(k-1)+t}x_{q(k-1)+t}\right\rangle + \tag{60}$$

$$+ \mathrm{diag}(\langle\psi_{k,t}\rangle)\Big)^{-1}, \tag{61}$$

$$\mu_{l_{k,t}} = \Sigma_{l_{k,t}}\left(\left\langle\upsilon_{q(k-1)+t}\right\rangle\left\langle\mathbf{x}_{q(k-1)+t}\mathbf{x}_{q(m-1)+t}\right\rangle\right), \tag{62}$$

$$\kappa_{k,t} = \kappa_0 + \frac{1}{2},\ t = 1, \ldots, q, \tag{63}$$

$$\nu_{k,t} = \nu_0 + \frac{1}{2}\left\langle l_{k,t}^2\right\rangle,\ k = 1, \ldots, (m-1), \tag{64}$$

$$\vartheta = \vartheta_0 + \frac{p}{2}, \tag{65}$$

$$\rho = \rho_0 + \frac{1}{2}\mathrm{tr}\left(\left\langle\mathbf{x}\mathbf{x}^T\right\rangle\mathbf{M}^T\mathbf{M}\right) - \mathbf{y}^T\mathbf{M}\langle\mathbf{x}\rangle + \frac{1}{2}\mathbf{y}^T\mathbf{y}. \tag{66}$$

The required moments of Gamma distributions are:

$$\langle\Upsilon\rangle = \mathrm{diag}\left(\left(\boldsymbol{\alpha}\circ\boldsymbol{\beta}^{-1}\right), \ldots, \left(\boldsymbol{\alpha}\circ\boldsymbol{\beta}^{-1}\right), \boldsymbol{\alpha}\circ\boldsymbol{\beta}^{-1}\right),$$

$$\langle\psi_{m,t}\rangle = \frac{\zeta_{m,t}}{\eta_{m,t}},\ t = 1, \ldots, q, \tag{67}$$

$$\langle\psi_{k,t}\rangle = \frac{\kappa_{k,t}}{\nu_{k,t}},\ k = 1, \ldots, m-1,\ t = 1, \ldots, q, \tag{68}$$

$$\langle\omega\rangle = \frac{\vartheta}{\rho}, \tag{69}$$

where symbol $\circ$ denotes Hadamard product (element-wise). The moments forming L_m are computed as

$$\langle l_{m,t}\rangle = \mu_{l_{m,t}}, \tag{70}$$

$$\left\langle l_{m,t}^2\right\rangle = \mu_{l_{m,t}}^2 + \Sigma_{l_{m,t}}, \tag{71}$$

and moments $\langle\mathbf{x}\rangle$, $\left\langle\mathbf{x}\mathbf{x}^T\right\rangle$, and $\langle l_{k,t}\rangle$, $\left\langle l_{k,t}^2\right\rangle$, $k = 1, \ldots, (m-1)$, are computed according to the truncated Gaussian distribution moments defined in 5.